BLEACHABLE ABSORBER LASER AMPLIFIER AND DETECTOR (BALAD)

Gordon Gould, et al

Polytechnic Institute of Brooklyn

Prepared for:

Rome Air Development Center
Advanced Research Projects Agency

23 October 1972

DISCLAIMER NOTICE

THIS DOCUMENT IS THE BEST QUALITY AVAILABLE.

COPY FURNISHED CONTAINED A SIGNIFICANT NUMBER OF PAGES WHICH DO NOT REPRODUCE LEGIBLY.

RADC-TR-72-313
Final Technical Report
October 1972

BLEACHABLE ABSORBER LASER AMPLIFIER AND DETECTOR (BALAD)

Polytechnic Institute of Brooklyn

Sponsored by
Defense Advanced Research Projects Agency
ARPA Order No. 1279
Amendment No. 2

Rome Air Development Center
Air Force Systems Command
Griffiss Air Force Base, New York

75R

Unclassified

Security Classification

DOCUMENT CONTROL DATA - R & D

(Security classification of title, body of abstract and indexing annotation must be entered when the overall report is classified)

1. ORIGINATING ACTIVITY *(Corporate author)*

Polytechnic Institute of Brooklyn
Route 110, Farmingdale, NY 11735

2a. REPORT SECURITY CLASSIFICATION

UNCLASSIFIED

2b. GROUP

3. REPORT TITLE

Bleachable Absorber Laser Amplifier and Detector (BALAD)

4. DESCRIPTIVE NOTES *(Type of report and inclusive dates)*

Final Tech Report 18 Nov 70 - 17 Nov 71

5. AUTHOR(S) *(First name, middle initial, last name)*

Gordon Gould
James T. Latourrette

6. REPORT DATE	7a. TOTAL NO. OF PAGES	7b. NO. OF REFS
23 Oct 72	75	25

8a. CONTRACT OR GRANT NO.

F30602-71-C-0024

b. PROJECT NO.

ARPA Order No. 1279, Amendment No. 2

c.

d.

9a. ORIGINATOR'S REPORT NUMBER(S)

PIBEP-72-107

9b. OTHER REPORT NO(S) *(Any other numbers that may be assigned this report)*

RADC-TR-72-313

10. DISTRIBUTION STATEMENT

Approved for Public Release. Distribution Unlimited.

11. SUPPLEMENTARY NOTES

Monitored by
Mr. William Quinn
RADC (OCTM-1), GAFB, NY 13441
AC 315 330-3030

12. SPONSORING MILITARY ACTIVITY

Advanced Research Projects Agency
Washington DC 20301

13. ABSTRACT

This final technical report was prepared by Polytechnic Institute of Brooklyn under Contract F30602-71-C-0024. It describes work performed at the Long Island Graduate Center, Farmingdale, N.Y. The principle investigators are Dr. Gordon Gould and Dr. James LaTourrette. Dr. Gould is also project engineer. This work is presently under continuation for an additional year under Contract F30602-72-C-0245, same title.

The Air Force Program Monitor is William C. Quinn RADC/OCTM-3.

ia

DD FORM 1 NOV 65 1473

Unclassified

Security Classification

14. KEY WORDS	LINK A		LINK B		LINK C	
	ROLE	WT	ROLE	WT	ROLE	WT
17-2-6-1						
17-2-6-2						
17-2-6-3						
17-5-1						
17-5-2						
20-5						
20-5-1						
20-6-5						

BLEACHABLE ABSORBER LASER AMPLIFIER AND DETECTOR (BALAD)

Gordon Gould
James T. LaTourrette

Contractor: Polytechnic Institute of Brooklyn
Contract Number: F30602-71-C-0024
Effective Date of Contract: 18 November 1970
Contract Expiration Date: 17 November 1971
Amount of Contract: $103,268.00
Program Code Number: OE20

Principal Investigator: G. Gould and J. T. LaTourrette
Phone: 516 694-5500

Project Engineer: G. Gould
Phone: 516 694-5500

Contract Engineer: W. C. Quinn
Phone: 315 330-3030

This research was supported by the Defense Advanced Research Projects Agency of the Department of Defense and was monitored by William C. Quinn RADC (OCTM-3), GAFB, NY 13441 under Contract F30602-71-C-0024.

1c.

PUBLICATION REVIEW

This technical report has been reviewed and is approved

William C. Quinn

RADC Contract Engineer

ABSTRACT

A detailed feasibility and design study has been made on the wide-angle, low noise BALAD receiver (Bleachable Absorber Laser Amplifier and Detector). Expressions have been derived for the achievable field-of-view, maximum gain and other specifications in terms of the dimensions and the measurable properties of the laser and absorber gases. Virtually error free detection is assured for signal pulses > 100 photons.

A figure-of-merit has been measured for several absorber gases screened from the literature. BALAD receivers with 4000 resolution element field-of-view are feasible using SF_6 and a CO_2 amplifier at 10.6μm and Xe with Xe at 3.5μm. The use of the latter is recommended for the experimental test of the BALAD receiver. Three compact absorber configurations have been considered and will be further investigated. Application is to optical radar and to optical communications where signal direction is uncertain.

TABLE OF CONTENTS

LIST OF FIGURES

LIST OF TABLES

1.0 SUMMARY

1.1 Objective

The objective of the subject contract is the investigation of Saturable Absorbers and their application to wide-angle, low-noise laser receivers.

1.2 Background

The combination of a Bleachable Absorber Laser Amplifier and a Detector (BALAD) as a receiver may have advantages over optical heterodyne or direct detection receivers, with respect to field-of-view, sensitivity, and bandwidth. In the BALAD concept the signal beam is amplified along with spontaneous emission from excited molecules in a laser pre-amplifier. The gaseous absorber is designed to saturate at an average intensity above the amplified spontaneous emission. Thus, the spontaneous emission and other background light is absorbed. The bleachable or saturable absorbing gas acts as an optical squelch suppressing the background radiation which does not coincide with the signal beam in direction, polarization, frequency and time. In addition, the signal beam of somewhat higher intensity is focused down on the absorber, "burns a hole" in it, and passes through with relatively little attenuation. Only light which is spatially coherent with the signal gets through to the detector.

Possible configurations for the receiver are shown schematically in Figs. 1, 2, and 3. The operation of the receiver is described in more detail in Sections 2.1 and 2.2.

1.3 Plan

In the subject one-year contract, the scope is limited to two tasks (line item A001):

Task 4.1.1: Screen the potentially useful absorbers in the 10.6μ and 3-5μ spectral ranges and measure the relevant properties of the most promising gases.

Task 4.1.3: Extend the feasibility and design study of the BALAD receiver.

1.4 Technical Problems, Methodology and Results

This report contains the detailed results of Task 4.1.1. These comprise the screening procedure used to select the best of the available absorbers, the detailed theory of the absorbers, and measurements of their relevant properties. The report also contains a summary of the results of Task 4.1.3 from which receiver performance can be predicted and physical design constants outlined. The details of the theory are contained in the previous report.[1] These results provide a basis for decisions on the future course of the program.

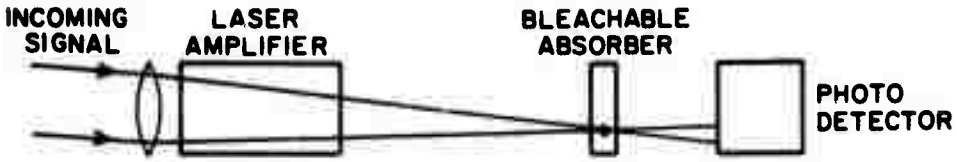

Fig. 1(a) - BALAD receiver. Absorber becomes transparent at the focus and frequency of the signal beam.

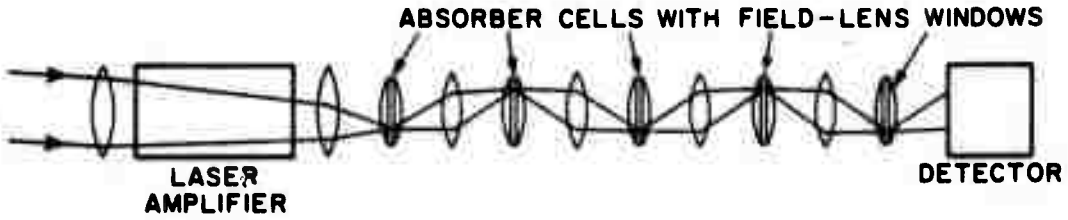

Fig. 1(b) - BALAD receiver with fine-focus multi-stage absorber required for gas with low attenuation and high saturation intensity.

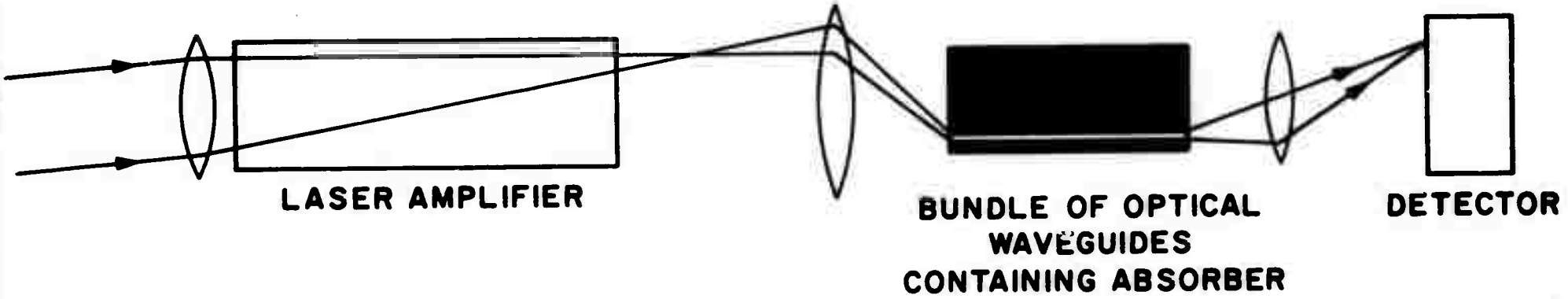

Fig. 2 - Alternative BALAD arrangement to that of Fig. 1. Periodic refocusing through absorber is unnecessary if light is confined in a waveguide.

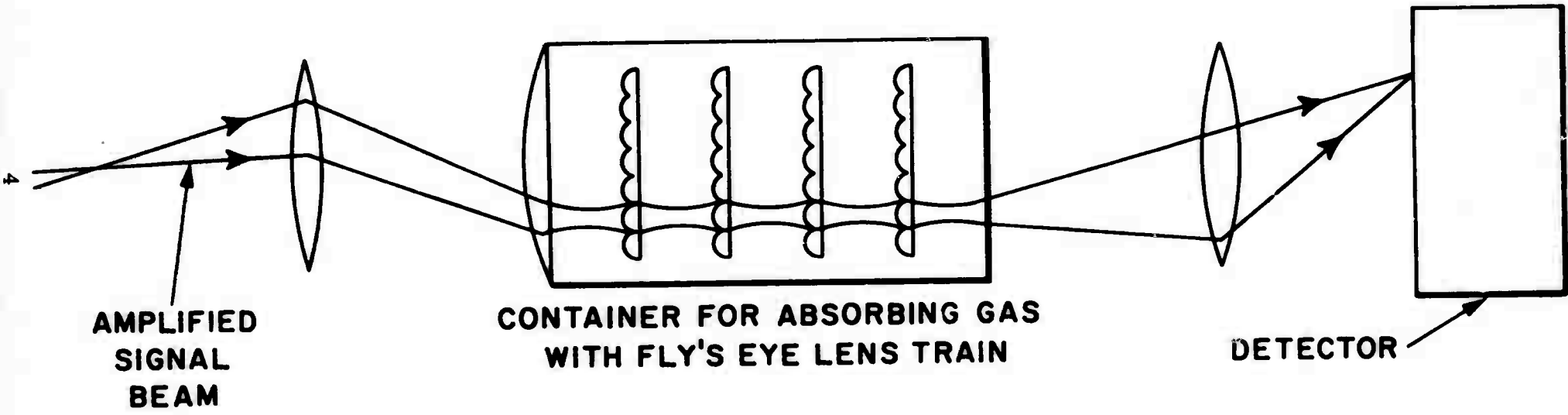

Fig. 3 - Alternative BALAD arrangement to Fig. 1(b). Fly's Eye lens train configuration. Focused signal beam is confined in absorber by series of lenslets in a molded fly's eye lens train. Each lenslet corresponds to a resolution element of the field-of-view.

1.4.1 Feasibility and Design Study

The most important questions addressed by this study are: (a) How large a field-of-view through the receiver is allowed by the actual characteristics of the best absorbers and by the technological and economic limitations on fabrication of the absorber configuration? (b) How small is the minimum signal which can be detected with satisfactory error rates?

(a) The principal advantage of the BALAD receiver over either direct detection or optical heterodyne detection of a radar or communication signal is this: BALAD can detect with maximum sensitivity a signal from any arbitrary direction in a sizeable field-of-view instead of having to close down the field-of-view to a single diffraction limited cone or resolution element.[2] It is therefore important to ask how large this field may be. For the configuration of Figs. 2 and 3, the maximum field-of-view through the receiver is given by (all quantities in MKS units):

$$\Omega_v \cong \frac{4.75 \times 10^{-25} \ell F_M}{[\varphi\lambda]\, a_m^2} \qquad (1)$$

where

$F_M \equiv$ figure-of-merit for the absorbing gas.

$\varphi \equiv$ branching ratio characteristic of the laser amplifier medium.

$\lambda \equiv$ wavelength.

$\ell \equiv$ path length through absorber.

$\pi a_m^2 \equiv$ minimum area of focal spot.

Thus, in addition to the limitations imposed by the laser and absorber media, Ω_v is limited by the smallness of technically or economically feasible optical waveguides or fly's eye lenslets for confining the focused signal beam. (See Sections 2.1 and 2.2).

A breakthrough has been achieved which removes the limitation on the field-of-view through the receiver. Recent advances in the state-of-the-art show high laser gain in small (0.5 mm diam) optical waveguides. Thus optical waveguides or a fly's eye lens train may be used to house both the amplifying and absorbing media. Up to 100 dB amplification is possible without saturation of the amplifier. This allows a very reasonable 0.5 mm diameter for the absorber guides. The only limitation on the number of resolution elements in this configuration is the acceptable size of the waveguide bundle. For example, a 200 x 200 array would be ~ 10 cm in diameter. The overall length is also shortened to between 1 meter (Xe-Xe) and 5 meters (CO_2-SF_6). The coupling optics are largely eliminated. Examples of possible receiver specifications are given in Section 5.2.

(b) The no-detection and false-detection error rates, other than those generated by circuit failure, arise at the input to the amplifier from photon fluctuations in the signal pulse relative to the spontaneous emission or "noise" pulse. It was shown in Ref. 1, Section 2.1.3, that the error rates primarily depend on the size of the average signal pulse and are little affected by other design considerations. The error rates rapidly become vanishingly small for signal pulses larger than 100 photons.

Another advantage of the BALAD receiver is that the absorber acts as a spectral filter which passes only the narrow band wherever it may fall. It is notable that the width of the signal band does not affect the achievable field-of-view. It does enter into other design parameters which may be calculated from the developed theory: path length through absorber, maximum output power, focused spot size, etc.

1.4.2 Investigation of Gaseous Absorbers

The figure-of-merit for absorbing gases,

$$F_M \equiv \left[\frac{\alpha_o B}{I_s}\right] \quad , \tag{2}$$

is discussed in Section 2.1. It is computed from measured values of the absorption coefficient, α_o, the saturation intensity, I_s, and the collision induced saturation bandwidth, B.

Two types of gaseous absorbers have been investigated:

(a) Unexcited molecules which absorb via vibration-rotation transitions within the well populated electronic ground state. The CO_2 laser transitions are of this type. These transitions are generally weak. The only absorbing transitions which have been found to overlap CO_2 laser transitions are of this type. The literature has been searched and a list of 75 potential absorbers in the 10.6μ meter and 3-5μm bands has been compiled. Rough absorption measurements reduced the list to two likely candidates, SF_6 and SiF_4. The figures-of-merit, F_M, were measured using apparatus designed and built in part under the contract. The best figure-of-merit was that of sulfur hexafluoride (SF_6) with $F_M = 3 \times 10^5$ meter/joules. An available review of vibration-rotation transitions in general suggests that a higher value of F_M is not likely to be found. (See Section 3.0.)

(b) Atoms which absorb via "allowed" transitions between electronic states excited or populated by an electric discharge. The high-gain $\lambda = 3.5\mu m$ laser transitions in xenon (Xe) is of this type. It can be made absorbing by over-driving the discharge. The figure-of-merit was measured to be $F_M = 5 \times 10^7$ m/j. It is likely that this can be further improved by variation of operating conditions. (See Section 4.0.)

1.5 Implications for DoD

A BALAD receiver for 10.6μm CO_2 laser signals with the specifications listed in Section 5.2 is feasible for application in an optical radar. Its usefulness would be to detect a target of uncertain position. For example, the receiver could be remote from the transmitter. It could also sensitively receive several separated signals simultaneously, or even an entire image.

A BALAD receiver utilizing xenon gas could function in a shorter range but higher resolution optical radar than the CO_2 system. This wide-angle receiver also could be utilized in a lightweight secure communication system.

1.6 Implications for Further R & D

(a) The fly's eye" and optical waveguide absorber configurations should be further investigated with a view to determining fabrication and experimental procedure.

(b) An experimental test of the BALAD receiver principle should be carried out using Xe-Xe media or CO_2-SF_6 media. The latter would be somewhat more expensive.

(c) An investigation should be made of techniques for filtering out spontaneous emission from all but the working CO_2 laser line.

2.0 FEASIBILITY AND DESIGN STUDY OF THE BALAD RECEIVER

Task 4.1.3 calls for "refining and extending the theory for more effective designs by taking into account the data and possible effects of the Investigation of Saturable Absorbers (Task 4.1.1). In particular, derive the necessary analytical expressions to determine performance, reliability, and cost estimates."

The desired analytic expressions governing the operation of the configuration in Fig. 1 were derived in the previous technical report.[1] They are summarized in Sections 2.1 and 2.2. The basic design equations relate maximum possible field-of-view through the laser amplifier, the receiver configuration and dimensions, the cross-sectional area of the focused signal beam, the required attenuation of background light, and the characteristics of amplifier and absorber gases. In particular, the maximum possible field-of-view is related to a figure-of-merit for the absorber.

The minimum detectable input signal pulse, on the other hand, is primarily determined by the required no-detection and false detection error rates. These, in turn, are limited by the shot fluctuations in successive signal pulses (and in the accompanying spontaneous emission from the amplifier which is spatially and spectrally coherent with the signal). Typically, the minimum detectable pulse will contain ~ 150 photons on the average.

2.1 Field-of-View Through Receiver

The BALAD receiver operates as follows: the signal is amplified and focused to a diffraction limited spot intense enough to saturate the absorber and pass through. Spontaneous emission from the first "gain length" of the amplifier is also amplified and focused into the various possible spatial propagation modes or focal spots. The parameters are adjusted so that the amplified spontaneous emission is just at the saturation intensity of the absorber (see Fig. 4).

The maximum amplifier gain is limited by saturation of the amplifier by the amplified spontaneous emission. Thus, the greater the field-of-view, the greater the number of resolution elements or modes, the smaller the maximum gain, and the smaller the required focal spot area. The maximum field-of-view then, is given by

$$\Omega_v \text{ (steradians)} \cong \frac{5.16 \times 10^{-24} s F_M}{[\varphi \lambda^2]} \quad , \tag{3}$$

where (all quantities are expressed in MKS units):

- s ≡ number of stages of refocusing through the absorber (see Fig. 1-b),
- λ ≡ wavelength,
- φ ≡ effective branching ratio of the amplifying medium,
- F_M ≡ a figure-of-merit for the absorber.

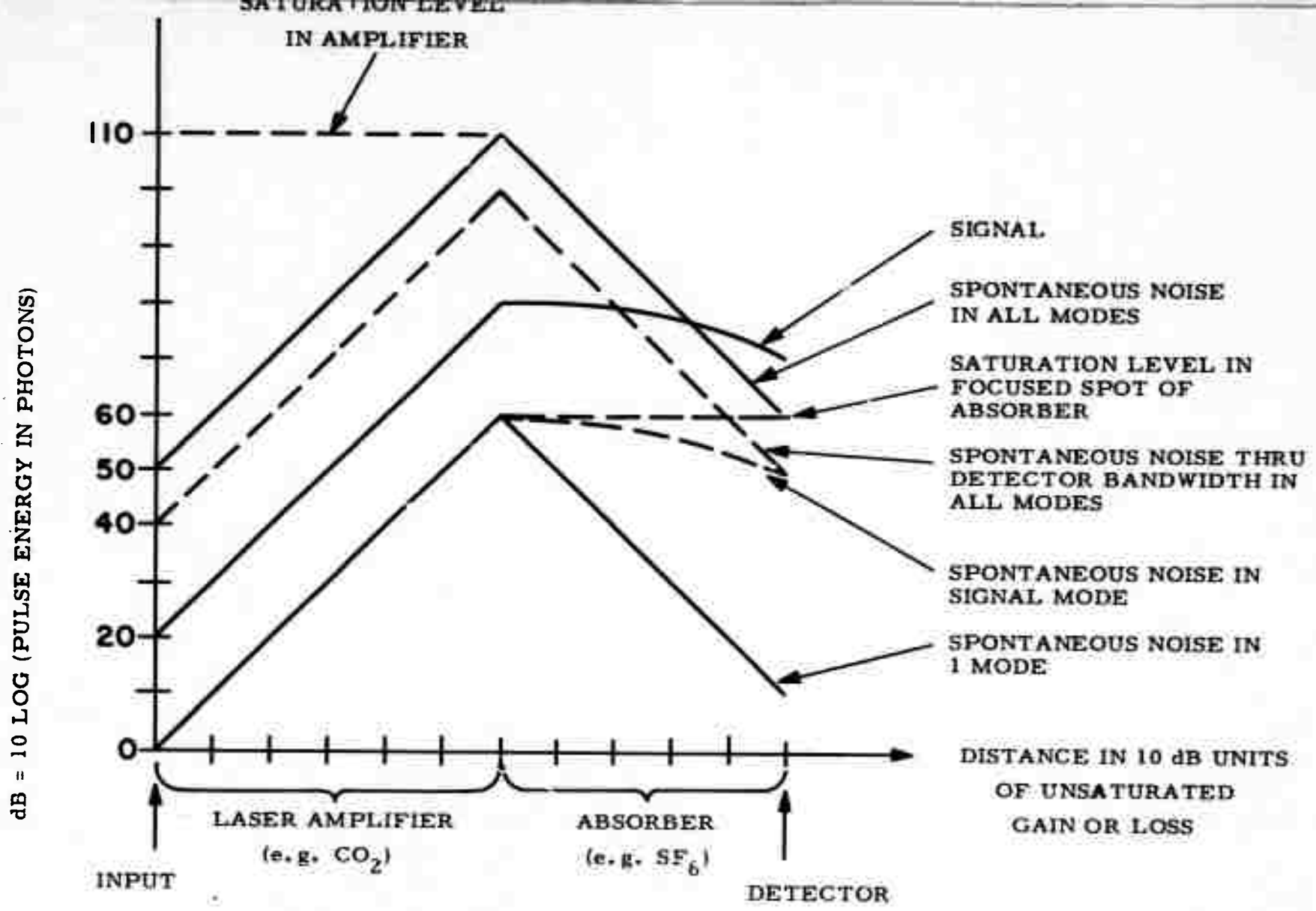

Fig. 4 - Typical evolution of signal and noise pulse energies on passing through the BALAD receiver. The spatial modes are cones leading to resolved focal spots. Post-detector bandwidth reduces the noise from its wideband value by $\sqrt{\frac{\text{signal band}}{\text{amplifier band}}}$.

$$F_M \equiv \left[\frac{\alpha_o B}{I_s}\right] \text{ in meters/joule} \quad . \tag{4}$$

This combination of unsaturated absorption coefficient ($\alpha_o \equiv \frac{1}{I}\frac{dI}{dz}$), bandwidth (B), and saturation intensity (I_s) is independent of pressure for passive absorbers such as SF_6. That is, F_M is independent of the collisional relaxation rate which determines the homogeneous or saturation bandwidth and which is to be matched to the signal bandwidth.

The field-of-view can also be expressed in diffraction limited-resolution elements or spatial modes, m:

$$\text{number of modes} \equiv m = \frac{405 \times 10^{-34} D^2 s F_M}{\varphi \lambda^4} \quad , \tag{5}$$

where D ≡ amplifier diameter. The number of resolution elements in the field-of-view is unchanged by the input optics.

The limitation on the field-of-view, due to saturation of the amplifier, may be circumvented by substituting an array of the recently demonstrated capillary amplifiers,[3,4] using the same geometry as will be discussed for the optical waveguide absorber configuration in Section 2.2. After ~ 10 dB of conventional amplification to counter insertion loss, the signal is focused on one or a few such amplifiers. Thus the spatial modes are isolated from each other. The amplified signal rather than the spontaneous emission then limits the single stage amplification to ~ 100 dB. A CO_2:He:N_2 mixture in a 1 mm i.d. glass tube exhibits an extraordinary gain of 24 dB/meter.[4] Thus the necessary amplifier length can be reduced to ~5 meters.

The observed saturating beam power (~ 10 watts) is ~50 dB greater than the signal power achievable by conventional amplification of a typical signal. It is more than sufficient to saturate an SF_6 absorber in a 1 mm diameter optical waveguide (see Section 2.2). Thus the two waveguide arrays can be matched and joined with minimal loss.

This configuration will be further studied during the second year of the program.

2.2 Absorber Configurations

The awkwardness of the multistage absorber configuration shown in Fig. 1-b can be avoided by arrangements which confine the signal beam to the focal spot size in the absorber. Figure 2 shows how this may be accomplished by a bundle of "optical waveguides." Each waveguide corresponds to a possible position of the focused signal spot or a resolution element in the field-of-view. Figure 3 shows how the same result may be accomplished by a train of "fly's eye lenses." In both cases, the length of the configuration is reduced to the actual required total path length through the absorber. Also the size of the components is reduced, making the configurations compact and economical.

The optical waveguide configuration makes possible a very small focal spot, and hence a usefully large field-of-view. This is made evident by reformulating the expression in Eq. (3) for the field-of-view in terms of the spot size:

$$\Omega_v = \frac{4.75 \times 10^{-25} \ell F_M}{[\varphi\lambda] a_m^2} \tag{6}$$

where

ℓ ≡ path length through absorber

πa_m^2 = minimum area of focal spot.

Again, the number of spatial modes in the field-of-view is given by

$$m = \Omega_v/\Omega \text{ (1 mode)} \tag{7}$$

or

$$m = \Omega_v \pi D^2/4\lambda^2 \quad .$$

The required absorber length is

$$\ell = [\text{dB (attenuation)}]/4.34\alpha_o$$

$$\simeq 12[\text{dB}]/\alpha_o \quad . \tag{8}$$

In one possible set of parameters for a CO_2-SF_6 BALAD receiver, as discussed in Section 2.2.3 of Ref. 1 yields an absorber length, $\ell \approx$ 2 meters.

The smallest usable optical waveguide and hence the largest achievable field-of-view, is determined by the acceptable signal loss in the waveguide wall. The minimum detectable input signal pulse is inversely proportional to this loss factor. In the previous technical report,[1] the classical loss rate in metal walls for the optimum mode (TE_{01}) was shown to be inversely proportional to the cross sectional area of the guide. For guide diameter of 100μ meter, the loss would be $\alpha(TE_{01}) \cong$ 2 dB/meter. For the CO_2-SF_6 BALAD parameters given in Section 2.2.3 of Ref. 1, the minimum signal would be raised by a tolerable factor of ~ 2. The field-of-view could then contain ~ 1000 resolution elements.

A further analysis of optical waveguide losses, especially mode conversion losses is recommended.

An array of small circular metal waveguides is a suitable configuration for containing a light beam in a passive bleachable absorbing gas such as sulfur hexafluoride (SF_6). It would not be feasible for an absorber such as atomic xenon, which must be excited by a discharge. For this case, a bundle of hollow dielectric waveguides is a suitable substitute.

It has been demonstrated that losses in the walls of a 0.4 mm glass capillary are $< 3\%$ per meter at $\lambda = 0.633\,\mu m$.[3,4] Using the scaling law of λ^2/a^3 for the losses, the attenuation at $\lambda(Xe) = 3.5\,\mu m$ would be a tolerable 3 dB per meter.

The gain in an active medium such as He-Ne or He-Xe confined in a 0.4 mm tube is several hundred dB per meter and inversely proportional to the diameter. This is primarily because the electron temperature is higher. Therefore the absorption in overdriven neon and xenon is also observed to be high. As described in Section 2.1, an array of dielectric waveguides containing the absorber can be matched to a corresponding array of amplifier capillaries. In this configuration the field-of-view is not limited by saturation, as in the case with a multimode amplifier.

The Fly's Eye Lens Train configuration is an alternative means for confining the signal beam to a small diameter as it passes through the absorber and/or amplifier (see Fig. 3). Each train of lenslets serves to guide a single propagating signal mode through the amplifier-absorber. This configuration is suited to transverse discharge excitation of amplifier and absorber media such as xenon gas. The propagation losses are not a serious problem, in the case of xenon, because of the high gain and attenuation coefficients. Both exceed 60 dB/meter for a wall spacing of 3mm.

The properties of modes propagating through a train of lenses have been thoroughly studied and have been summarized by Yariv.[5] The diffraction losses per pass through a lens, are a function of the Fresnel number, N:

$$\text{Fresnel No.} \equiv N \equiv \frac{a^2}{d\lambda} \tag{9}$$

where

$2a \equiv$ lens diameter

$d \equiv$ lens spacing .

For a lens curvature corresponding to a "confocal" configuration, the loss is $< 0.1\%$ per pass for the lowest order mode with $N \sim 1$. The cross sectional "area" of this mode at the lens (to $1/e^2$ power points) is[5]

$$\text{mode cross section} \equiv \pi w_o^2 = d\lambda \quad . \tag{10}$$

The focal spot diameter at the entrance should be made twice the lens diameter to ensure excitation of one mode through a two-dimensional hexagonal close-packed array of lenslets. Then the insertion loss can be estimated at $\sim 90\%$. This can be made up by 10 dB of conventional coherent preamplification, to avoid an increase in the statistical fluctuations of signal pulses.

Reasonable dimensions based on the considerations given above are:

wavelength, λ	=	3.5 μm for xenon
lenslet spacing	=	3mm
lenslet dimensions	=	0.2mm
length		
amplifier train	=	1 meter
absorber train	=	1 meter
no. of fly's eye lenses	=	600
transverse dimensions	=	10cm for 500 x 500 element field

The key to economic and technical feasibility in fabricating this configuration lies in molding the identical fly's eyes with a precision die. A material suitable for the 3.5 μmeter wavelength region is arsenic trisulfide glass (As_2S_3). Lenses of this material are molded by several companies. The refractive index is high (n = 2.3), making possible single layer low reflection coatings. If the Fresnel reflections per lens can be kept below 0.5%, receiver performance will not suffer. These considerations warrant further study.

2.3 Propagation of Pulses through a Saturated Absorber

In order to design the BALAD receiver, it is desirable to be able to quantitatively analyze the characteristics of signal pulses propagating through a saturable absorber. During this report period we have not been able to incorporate all of the significant features of realistic saturable absorbers in our analysis. We were, however, able to demonstrate the feasibility of taking into account effects which had not been previously analyzed. Thus a straightforward extension of our work will enable us to make quantitative evaluation of the effect of propagation distortion on system performance. One of the important factors still to be included is the effect of degeneracy. It is expected[6] that this effect will tend to diminish the importance of coherent effects such as longitudinal pulse break-up and extend the range of validity of a rate equation approach.

The pertinent quantities to be determined are the temporal and spatial variations of the pulse as a function of the absorber length and characteristic relaxation times. The analysis must be carried out for a range of situations such that nonlinear saturation effects become important. These may include the phenomena of longitudinal and transverse pulse break-up, which could have serious implications for the operation of BALAD. General analytical techniques which are useful for linear problems, are not applicable over the nonlinear range and it is necessary to resort to numerical methods. The literature contains investigations which have been suggestive of important phenomena, but not directly relevant to the situation of interest for our application. In particular, the development of transverse structure in propagating pulses has not been sufficiently analyzed. If the pulse shape is significantly altered, as a result of propagation through

the resonant medium, the magnitude of the minimum detectable signal will be raised. The signal is partly determined by the amount of spontaneous emission noise from the pre-amplifier reaching the detector. If the transverse dimensions of the pulse increase, more modes excited by spontaneous emission from the pre-amplifier will penetrate the absorber and reach the detector. If the time duration of the pulse increases, the integrated noise power increases. The development of phase variations can affect the focusing properties of the pulse, and hence the performance of the multifocused absorber configurations. This study is aimed toward the quantitative evaluation of these phenomena and the determination of the effect on system performance. In this report, we will discuss our formulation of the problem and some of our preliminary results.

During this report period we have been studying the development of the longitudinal and transverse pulse shape as a function of the propagating path through an absorbing medium. Because the coupled field-material system equations are nonlinear, general analytic expressions cannot be given for the propagation of arbitrary input pulses. Analytical solutions have been obtained for certain classes of distortionless pulses in particular types of media.[6] Also, useful theorems for the propagating characteristics of the area under the pulse amplitude have been derived by McCall and Hahn.[7] They later extended their study[8] to include transverse geometrical and degeneracy effects. In their analysis the transverse field variations are assumed, rather than solved for. Numerical procedures useful for problems in which there is no spatial variation in direction transverse to the propagation direction have been developed by Hopf and Sculley[9] and Icesevgi and Lamb.[10]

In our work, we are interested in determining the effect of transverse field variations such as would develop from arbitrary input pulses onto an absorbing medium. One class of input pulses of particular interest are those with quadratic phase variation over the input plane. These would represent focused waves in the absence of the saturable absorbing medium. The results we will report are based on numerical integration of the coupled field-material system equations.

2.3.1 Field and Material System Equations

The field is assumed to be linearly polarized transverse to the direction of propagation, the z direction. It is taken to be of the form:

$$E = \mathcal{E} e^{-i\theta} + \text{complex conjugate} \tag{11}$$

with

$$\theta = \omega t - \frac{\omega n z}{c} \quad , \tag{12}$$

where n is the index of refraction associated with the non-resonant part of the material system. The resonant part of the material polarization is taken to be of the form

$$P = (-i)\mathcal{P}e^{-i\theta} + \text{complex conjugate} \quad . \tag{13}$$

Using the slowly varying wave approximation and assuming that the transverse scale of the pulse is small compared to the longitudinal scale, the wave equation becomes:

$$[i\frac{c}{\epsilon n\omega}\partial^2/\partial_y^2 + \partial/\partial z + \frac{n}{c}\partial/\partial t]\mathcal{E} = \frac{2\pi\omega}{nc}\mathcal{P} \quad . \tag{14}$$

At this stage of our study we have found it convenient to deal with a geometry corresponding to no spatial variation along one transverse (x) direction. We will discuss at the end of this section the generalization to a rotationally symmetric (about the z axis) geometry.

The resonant part of the material polarization is the sum of contributions from molecules with different central frequencies (inhomogeneous broadening) and dipole moments (degeneracy). Indicating the degeneracy by the index j, and the distribution of central frequencies by the function $g(\Delta)$, with Δ equal to the difference between the atomic resonance central frequency and the frequency of the carrier ω, we have

$$\mathcal{P} = \sum_j N_j \int g(\Delta) P_j(\Delta)\, d\Delta \quad , \tag{15}$$

where N_j is the density of the degenerate species. The complex polarization $P_j(\Delta)$ of the two level system of central resonant frequency $\omega_a = \omega + \Delta$, and dipole matrix element μ_j satisfies the Bloch equations:

$$(\partial_t + \frac{1}{T_2} + i\Delta)P_j = \frac{\mu_j^2 \mathcal{E}}{\hbar} W_j \tag{16a}$$

$$(\partial_t + \frac{1}{T_1})(W_j - W_{j,o}) = -\frac{2}{\hbar}(\mathcal{E}P_j^* + \mathcal{E}^* P_j) \quad , \tag{16b}$$

where T_1 and T_2 are the longitudinal and transverse relaxation lines, respectively, and $W_{j,o}$ is the steady state population difference in the absence of the applied field.

The work described in this report is limited to the case of a pair of nondegenerate levels and a homogeneous line. For this case, it is convenient to deal with the following dimensionless equations:

$$(-i\Gamma\partial_y^2 + \partial_z + \beta\partial_t) = \mathcal{P} \tag{17a}$$

$$(\partial_t + 1)\mathcal{P} = W \tag{17b}$$

$$(\partial_t + \frac{T_2}{T_1})(W - W_o) = -2(\mathcal{E}\mathcal{P}^* + \mathcal{P}^*\mathcal{E}) \quad , \tag{17c}$$

where

$y \leftarrow y/y_o$ (the transverse dimension is measured in units of the transverse aperture, y_o)

$t \leftarrow t/T_2$ (the time is measured in units of the "transverse" relaxation time, T_2)

$z \leftarrow \alpha_o z$ (the longitudinal distance is measured in units of unsaturated absorption length, α_o^{-1})

$\mathcal{E} \leftarrow \frac{\mu}{h} T_2 = \sqrt{\frac{I}{I_s}}$ (the field is measured in units of the saturation intensity).

The dimensionless parameters which enter into Eqs. (17) are

$$\beta = \frac{n}{cT_2\alpha_o} = \frac{\text{absorption length}}{\text{distance travelled by light in time } T_2}$$

$$\Gamma^{-1} = \left(\frac{2n\omega\alpha_o y_o^2}{c}\right) = \text{Fresnel number corresponding to aperture } y_o \text{ and distance } 1/\alpha_o$$

$$T_2/T_1 = \text{ratio of transverse to longitudinal relaxation times}$$

$$W_o = \text{Fractional unsaturated population inversion, } \frac{N_1 - N_2}{N_1 + N_2} \text{ for } \mathcal{E} = 0 .$$

Variations in transverse structure occur because of the second order y derivative in Eq. (17a). For $\rho = 0$ this is the term responsible for diffraction. For $\Gamma = 0$ (one dimensional propagation) solutions exist for which $\mathcal{E}$ and ρ are real (no phase modulation). The presence of transverse variations is associated with phase modulation. A new feature of our work is the inclusion of this term in the numerical analysis of pulse propagation.

2.3.2 Results of Numerical Calculations

In this section, preliminary results of numerical integration of Eqs. (17a-c) for several interesting sets of parameters are described. The wavelength assumed is 10μ and the transverse structure of the input field is assumed gaussian with 1 cm half width. The time dependence of the input pulse is assumed, in these calculations, to be $\operatorname{sech} t/T_p$, and the incident amplitude is described in terms of the input area

$$A = \int_{-\infty}^{\infty} (\mu\mathcal{E}/\hbar)(t)\, dt \quad .$$

We have taken the absorption length, α_o^{-1}, to be 15 cm for T_2 = 10 nsec.

In Figs. 5(a) and 5(b) are plotted the longitudinal and transverse variations of a pulse with input area A = 2π (a so-called "2π pulse"). In this case and all other figures showing transverse variation the field is symmetric about the mid-plane marked y = 1, and is calculated for the instant that the field at this plane has its maximum value. In Figs. 5(c) and 5(d), we note the longitudinal and transverse behavior after 90 cm of propagation path for the case $T_1 = T_2 = \infty$. By this distance there is considerable transverse structure. This transverse pulse break-up is associated with the fact that the structure in the various transverse planes moves with different velocities.

The effect of introducing finite relaxation times is shown in Figs. 5(e) and 5(f). This gives the longitudinal and transverse structure after 90 cm for the same 2π input pulse just discussed, but for the case $T_1 = T_2 = 10$ nsec. The development of longitudinal structure is again evident. However, in this case the dominant peak in each transverse plane moves with the same velocity (very close to c/n). Thus the transverse structure remains smooth and does not show transverse break-up. The effect of focusing in one dimension is illustrated in Fig. 6. The longitudinal and transverse variations of the input pulse are shown in Figs. 6(a) and (b), respectively. The phase variation over the input aperture is such as to lead to focusing. In the absence of the medium, the effect of focusing is shown in Figs. 6(c) and 6(d) where we have shown the time and transverse space variation in the focal plane. We note the focusing of the input field. The effect of the medium on the focused pulse characteristics is shown in Figs. 6(e) and 6(f) which show the temporal and transverse space variations in the focal plane for the case $T_1 = T_2 = T_p$.

Preliminary Conclusions and Recommendations

We have demonstrated the feasibility of taking into account the transverse structure in numerical calculations of pulse propagation. However, our results, so far, apply only to a non-degenerate, homogeneous line. Because of these limitations only the following preliminary conclusions can be drawn at this time. When the pulse duration is short compared to the relaxation times, transverse, as well as longitudinal break-up can occur. As the relaxation times are shortened, the longitudinal variations of the various transverse planes become synchronized, and a transverse cross-section may not show structure, even though longitudinal structure has developed in each transverse plane. The effect of focusing in the presence of a saturable absorber has been investigated. An effective sharpening of the pulse was seen to occur.

A more realistic model must include the effects of degeneracy and Doppler width. We have been able to extend our numerical program to include these effects. Also, we can easily adapt this program to describe the interesting case of a rotationally symmetric geometry, simply by replacing Eq. (14) by the equation:

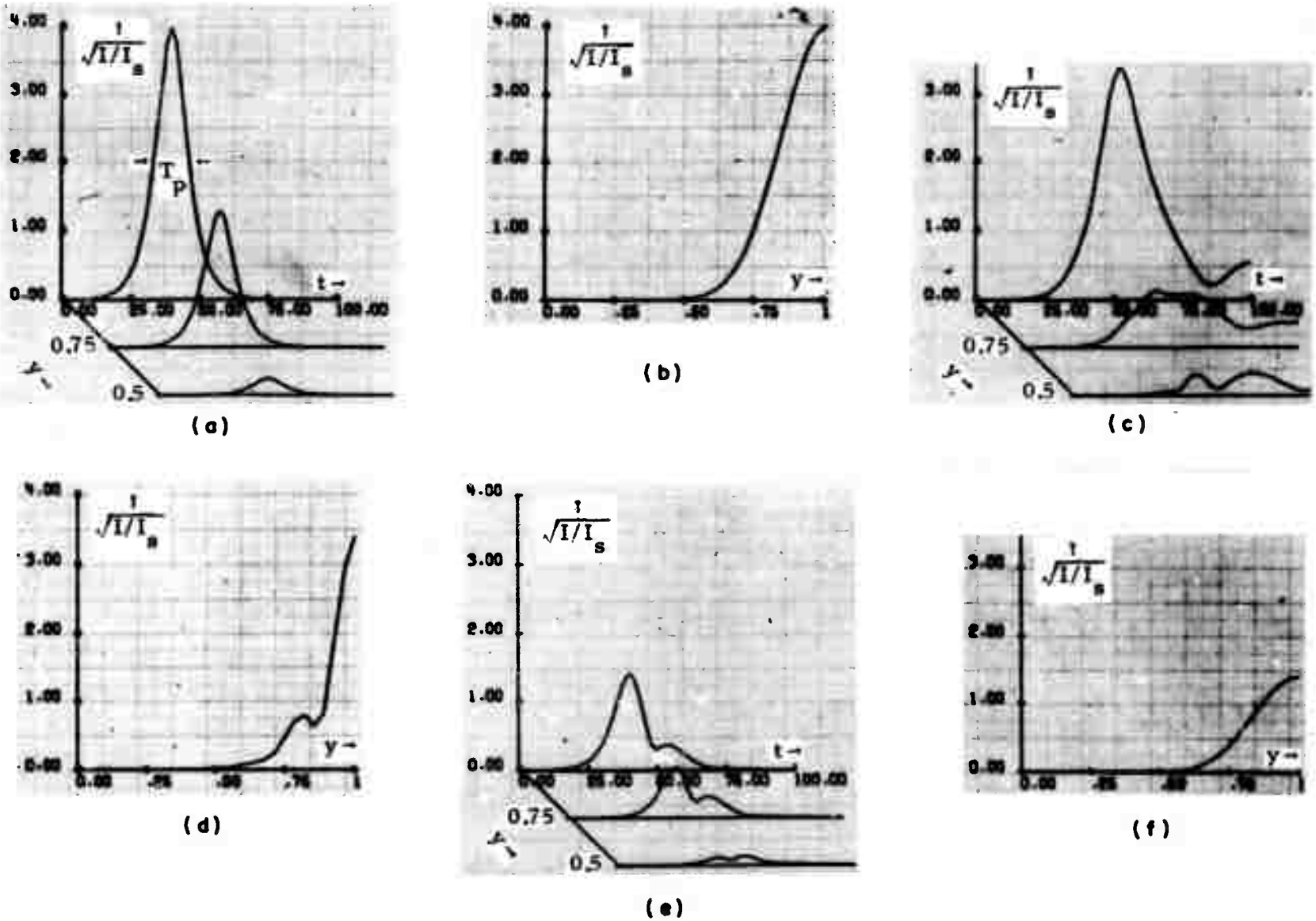

Fig. 5. Illustrating the transverse variation of a propagating pulse. "Area" = 2π in central plane. (a) Temporal variation for three transverse planes. (b) Input transverse spatial variation at single time. (c) Temporal variation after propagation - pulse duration short compared to relaxation times. (d) Transverse spatial variation after propagation - pulse duration short compared to relaxation times. (e) Temporal variation after propagation - pulse duration comparable to relaxation time. (f) Transverse spatial variation after propagation - pulse duration comparable to relaxation time.

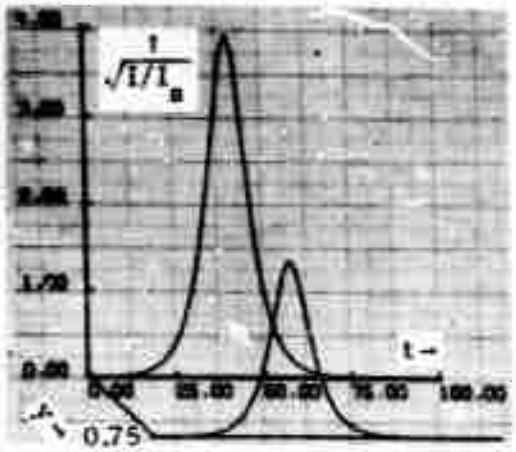

(a)

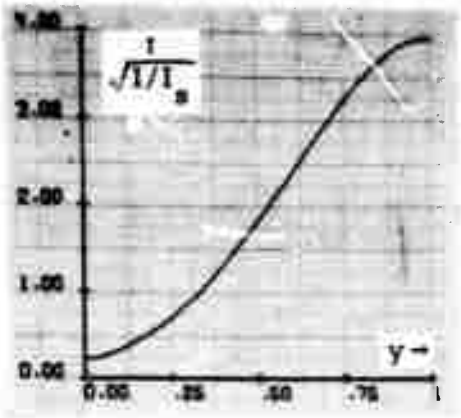

(b)

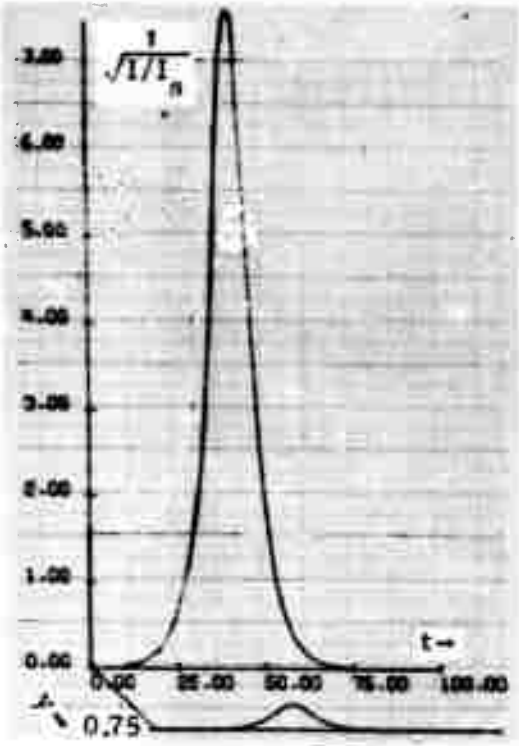

(c)

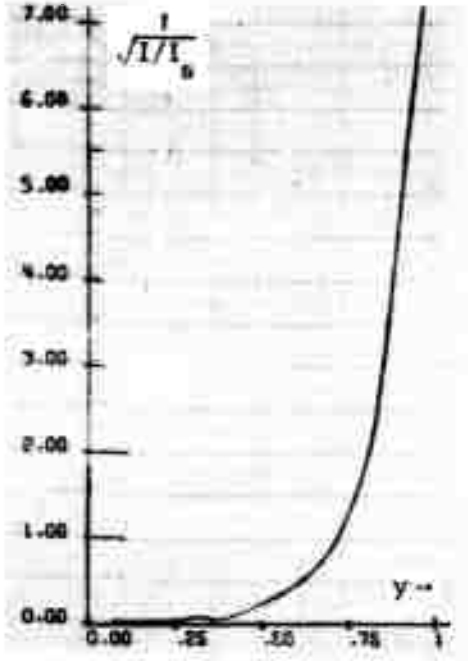

(d)

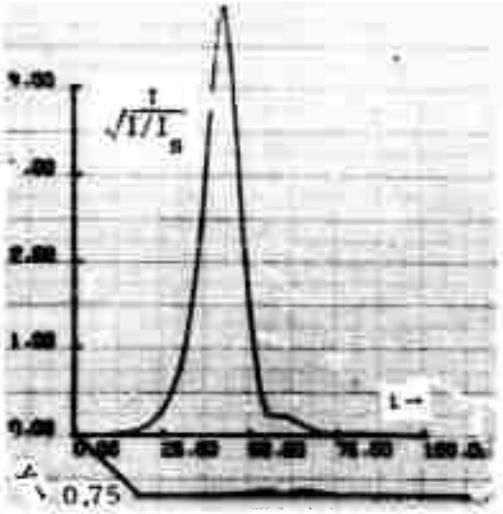

(e)

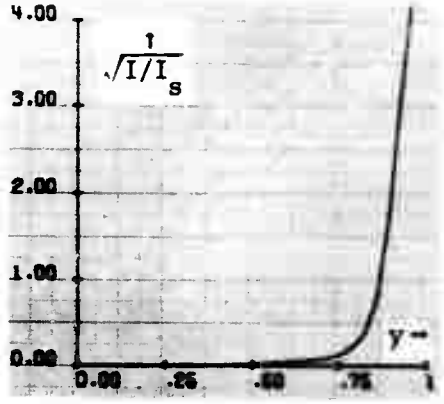

(f)

Fig. 6. Effect of focussing a pulse which has "area" equal to 2π in the central plane. (a) Input temporal variation for two transverse planes. (b) Input transverse spatial variation at single time. (c) Temporal behavior in focal plane - no absorber. (d) Transverse spatial behavior in focal plane - no absorber. (e) Temporal behavior in focal plane - with absorber. (f) Transverse spatial behavior in focal plane - with absorber.

$$\left[-i\frac{c}{2n\omega}\left(\frac{\partial^2}{\partial\rho^2}+\frac{1}{\rho}\frac{\partial}{\partial\rho}\right)+\frac{\partial}{\partial z}+\frac{n}{c}\frac{\partial}{\partial t}\right]\mathcal{E}=\frac{2\pi\omega}{nc}\mathcal{P} \quad . \tag{18}$$

The only new variable in this equation is ρ the transverse radial coordinate. We recommend the continuation of this analysis, which should now be a reliable model from which quantitative conclusions relative to the performance of the BALAD receiver can be drawn. The conclusion of most interest is how much, if at all, the signal pulse energy must be increased to achieve the expected performance.

3.0 PASSIVE MOLECULAR ABSORBERS

In this section the absorption properties of vibration-rotation transitions in molecules are discussed in relation to the selection of molecules as saturable filters for the BALAD receiver. A table of potential absorbers together with relevant information from a literature search is included. The experimental procedure for determining the absorption properties of selected molecules is described and the experimental results obtained with four gases are presented.

3.1 Theory of Molecular Absorbers

The properties of molecular absorbers that are relevant for their use as saturable filters are (1) the resonant frequency, (2) the absorption bandwidth, (3) the absorption coefficient, (4) the saturation intensity and, (5) the gas temperature. An ideal molecular absorber should be resonant at the same frequency as the amplifier and have a bandwidth as great or greater than the amplifier to completely mask spontaneous emission noise generated by the amplifier. The absorption coefficient should be large enough to provide operation with a relatively short column of material, and the saturation intensity should be sufficiently low so that bleaching of the absorber occurs at input intensity levels not much greater than the spontaneous emission level from the amplifier. The temperature of the absorber must be low enough so that broad band thermal radiation is small compared with the spontaneous emission of the amplifier. In the semi annual report,[1] a figure-of-merit for an absorber was derived in terms of these parameters. This is expressed as the ratio $F_M = (\alpha_o B/I_s)$, where α_o is the line center absorption coefficient, B, the molecular bandwidth, and I_s is the saturation intensity. The dependence of these quantities on the physical properties of the absorber will be considered.

It should be noted that in general these quantities cannot be calculated, but must be measured. Primarily because of the large uncertainty in frequencies of molecular vibrational band centers, it is not possible to know which fine structure component of a given band overlaps the laser bandwidth.

Aside from the question of overlap, the figure-of-merit is generally a complicated function of basic molecular properties such as: molecular weight, moment of inertia, dipole matrix element, rotational angular momentum, collision cross-section and temperature. However, the most significant factor is the dipole matrix element. This quantity enters quadratically in the absorption coefficient and, as we will also show, appears as inverse square in the saturation intensity. As a result, F_M, the figure-of-merit, is proportional to the fourth power of the transition matrix element.

For any particular absorption transition that is coincident with a laser frequency, it is not possible to know the matrix element without detailed spectroscopic information. This, in general, can only be obtained through experiment. At the start of this program, we assembled a list of potential molecular absorbers for the BALAD program. This list is presented in Section 3.1.8. When the list was organized, the only indication of transition strengths were qualitative remarks from the references. Since then, we have found one particular reference that has quantitative values of band strengths, from which approximate dipole mounts may be deduced. This reference is a monograph by L. A. Gribov entitled "Intensity Theory for Infrared Spectra of Polyatomic Molecules."[11] Gribov lists the integrated band strengths for several hundred vibrational transitions. These values are proportional to the square of the dipole matrix element. However, any particular rotational transition within a vibrational band will have its matrix element altered by factors which depend on the molecular structure and the rotational quantum numbers and degeneracies associated with the transition. As a result, the values presented can be used only for a first order selection of molecular absorbers for BALAD. Of those molecules listed which have transitions in the 10μ range, SF_6, and SiF_4 have the largest absolute intensity, with SF_6 almost twice as large as SiF_4. Methylfluoride CH_3F and Ammonia NH_3, which we assumed would be strong candidates as saturable absorbers have only 10% of the SF_6 intensity. Another rather surprising fact is that of all transitions listed, over all wavelengths, the ν_3 transition of SF_6 is the strongest. These results have been qualitatively verified from the measurements that have been completed on SiF_4, SF_6, Methyl Alcohol, and Methylfluoride as listed in Section 3.1.8. These facts strongly suggest that a molecular absorber for the 10.6μ region with better characteristics than SF_6 will not be found. However, in the 3-5μ region, OCS, which is a linear molecule, has a transition intensity comparable with SF_6 and should be examined.

3.1.1 Absorption-Coefficient

The absorption coefficient at line center for a Doppler broadened line is given by

$$\alpha_o \approx \frac{\lambda^2 A_{21} N_1}{8\pi \Delta\nu_d} \frac{g_2}{g_1} \tag{19}$$

where we have assumed the upper level to be empty; A_{21} is the Einstein spontaneous emission coefficient which is proportional to the square of the dipole matrix element, N_1 is the lower level population, g_2/g_1 is the ratio of the upper to lower level degeneracies, and $\Delta\nu_d$ is the Doppler width of the transition.

In general, the dipole matrix elements for strong molecular vibration-rotation transitions are of the order $\approx 3 \times 10^{-19}$ esu, leading to spontaneous emission rates of

about 30 sec^{-1} at $\lambda = 10\mu$. However, matrix elements are known only in very special cases and not calculable for molecular transitions where the rotational sublevels are unspecified. The ratio of the degeneracies g_2/g_1 depends on the specific rotation-vibration transition and is near unity for high values of the rotational quantum number, J. The Doppler width, $\Delta\nu_d$, can be specified exactly and is proportional to $(T/M)^{1/2}$, where T is the temperature and M is the molecular weight. Although the absorption coefficient is inversely proportional to the Doppler width, the bandwidth of absorption required by BALAD must be equal to or greater than that of the amplifier, so that a massive molecule is in general less desirable than one having a molecular weight comparable to the source, e.g., CO_2. The exception is a molecule for which a high density of absorption lines cover the desired bandwidth. This is the case with SF_6.

The number of molecules in the lower state, N_1, depends on several factors. We have considered only ground state transitions because at ambient temperatures or below the bulk of the population is found in the ground vibrational level. For example, the CO_2 laser transition which may also be driven to absorption is omitted although the overlap in that case would be perfect. The reason is that the absorption obtainable at useful temperatures would be too small.

The ground level population is in general divided among a large number of rotational sublevels as determined by the rotational partition function. The number of rotational levels that have a significant fraction of the population at a given temperature depends on the energy spacing between rotational levels which in turn is inversely proportional to the moment of inertia of the molecule. Since one would like to maximize the number of molecules per absorbing state, we prefer a small moment of inertia, so that the population of the ground vibrational level would be distributed over only a small number of rotational sublevels. Thus, all other factors being equal, a light molecule with a small moment of inertial would in general be a stronger absorber than a heavier one. One difficulty is that with fewer rotational sublevels, the probability of a good coincidence is small. Another element that determines the number of absorbers per sublevel is the splitting of degeneracies. As an example, a spherical top molecule has a $(2J+1)^2$ degeneracy associated with each rotational level as compared with a $(2J+1)$ degeneracy for a linear molecule.[12] For the spherical top, part of the degeneracy may be removed by Coriolis interaction, resulting in a further spreading of the transition strength over the additional rotational fine structure. In SF_6, the excellent overlap with a number of CO_2 transitions can be accounted for in this way.[13] Although this effect leads to a higher probability of finding an overlap, it is basically undesirable because the absorption strength is spread over too great a frequency range. In general, a molecule with simple structure and a minimum of atomic components such as a diatomic molecule is preferable to a more complex structure.

3.1.2 Temperature Variation of Absorption

The absorption coefficient at line center for a Doppler broadened line is given by Eq. (19) where it was assumed that the upper level was empty. In this expression only the quantities $\Delta\nu_d$ and N_1 are functions of the temperature. The Doppler width which depends on the mean velocity of the particles is proportional to $T^{1/2}$. The population of the particular rotational sublevel involved in the absorption of the laser radiation depends in a complex way on the temperature. For a heavy spherical molecule such as SF_6 or SiF_4, the population of a particular rotational level is given by the product of the Boltzmann factor and level degeneracy which may be written as

$$n_J \cong n_o(2J+1)^2 \exp[-\beta J(J+1)hc/kT] \tag{20}$$

where β is the rotational constant.

For $\beta hc \ll kT$, the total population of the vibrational level N, can be found by integrating n_J over J, taking J as a continuous variable, thus, replacing the sum over J by an integral. This gives

$$N \cong n_o \pi^{1/2}(\beta hc/kT)^{-3/2}[1 - \mathrm{Erf}\{\tfrac{1}{2}(\beta hc/kT)^{1/2}\}]\exp(\beta hc/4kT) \quad . \tag{21}$$

For SF_6, $\beta = 9 \times 10^{-2}\,cm^{-1}$,[13] and in the temperature range from 100°K to 300°K, the quantity $(\beta hc/kT)$ is less 1.5×10^{-3}. As a result, the Erf can be neglected in comparison to unity and one obtains the following expression for the population of J_{th} rotational level

$$n_J = N(2J+1)^2(\beta hc/kT)^{3/2} \exp\{-\beta hc(J+\tfrac{1}{2})^2/kT\} \quad . \tag{22}$$

The variation with temperature of the absorption of the CO_2P(16) line which is of primary concern in the BALAD program can be estimated by using the fact that this transition has a J value of ten or less.[14, 15] This result in the exponential factor being close to unity so that the total variation in n_J is proportional to $NT^{-3/2}$. At constant pressure N is approximately inversely proportional to T, for pressures below the saturated vapor pressure. The net dependence on temperature including the Doppler width produces a T^{-3} variation of the absorption coefficient for the SF_6 transition coincident with the CO_2P(16) laser line.

For linear molecules such as CO_2 in which the energy separation between the rotational levels is small compared to thermal energies the number of molecules in a given rotational level is given by [12]

$$n_J \approx N \frac{hc\beta}{kT}(2J+1)\exp\{-\beta J(J+1)hc/kT\} \quad . \tag{23}$$

This produces a net dependence on temperature of $T^{-5/2}$ for low J transitions.

3.1.3 Saturation Intensity

The saturation intensity can be derived from a theoretical consideration of the response of a two level homogeneous system to a strong monochromatic field. The steady state expression for the population difference found by the rate equation approximation is given by

$$\Delta N = \frac{\Delta N_o}{1 + 2T_1 T_2 (\mu \cdot E/h)^2} \tag{24}$$

where T_1 is the population relaxation time, T_2 is the phase relaxation time, μ is the dipole matrix element, and E the electric field intensity. The saturation intensity is defined as that value of E^2/Z_o for which the zero field population difference is reduced in half. $Z_o = \sqrt{\mu_o/\epsilon_o}$ is the free space wave impedance. We can then rewrite the equation as

$$\Delta N = \frac{\Delta N_o}{1 + I/I_s} \quad , \tag{25}$$

where I_s is the saturation intensity. Since the absorption coefficient depends linearly on population difference, this may be expressed as

$$\alpha = \frac{\alpha_o}{1 + I/I_s} \quad . \tag{26}$$

For the case of inhomogeneous broadening as produced by the Doppler effect, it can be shown that when the Doppler width, $\Delta\nu_d$, is much greater than the homogeneous width, $\Delta\nu_h$, the resulting expression for the absorption coefficients obtained by integration over velocity is given by

$$\alpha(\omega) = \frac{\alpha_o(\omega)}{(1 + I(\omega)/I_s)^{1/2}} \tag{27}$$

where ω is the optical frequency. This result is based on the assumption that each molecular velocity group may be treated independently. That is, that the cross-relaxation rate between velocity groups as a result of collisions is small compared with other relaxation rates.

The saturation intensity

$$I_s = h^2/2T_1 T_2 \mu^2 Z_o = h^2 c \epsilon_o / 2\, T_1 T_2 \mu^2 \quad , \tag{28}$$

depends inversely on the three parameters T_1, T_2, and μ^2. For allowed vibration-rotation transitions, values of μ of about 10^{-19} esu are typical, and one notes that

large dipole matrix elements are correlated with strong absorption lines. The population relaxation rate, T_1^{-1}, is the sum of several different rates of differing pressure and temperature dependence. Diffusion of molecules out of the beam, spontaneous emission, collisional de-excitation of the rotational and vibrational levels, all contribute to determining the value of T_1. The rate of diffusion is inversely proportional to pressure while the rate of spontaneous emission is constant and collisional de-excitation is proportional to pressure. However, for the experimental conditions appropriate to the BALAD receiver, the dominant effect in the molecules examined is due to collisional de-excitation of the rotational levels and T_1^{-1} is proportional to pressure. For molecular vibration-rotation transitions, T_2, the phase interruption time, is also determined primarily by kinetic collisions. Each collision produces a phase interruption and to a high probability a change in rotational state of the molecule as well. This results in T_1 and T_2 being nearly equal, with T_1 somewhat larger.

In terms of kinetic properties, the collision rate is given by

$$R = \frac{1}{T_2} = N\sigma \bar{v}_{rel} \tag{29}$$

where N is the gas particle density, σ is the effective cross-section, and $\bar{v}_{rel}$ is the mean relative velocity of the colliding particles.

If one makes the assumption, that σ, the collision cross-section is a slowly varying function of temperature and notes that $n\bar{v}_{rel}$ is proportional to the product $PT^{-1/2}$, one concludes that the saturation intensity which is proportional to $(1/T_1T_2)$, varies as P^2T^{-1}, where P is the pressure and T the temperature.

3.1.4 Effects of Degeneracy

The high level of degeneracy frequently associated with molecular transitions, can radically alter the expression for the saturation intensity as well as the absorption coefficient. Basically with degeneracy present, the transitions can be thought of as consisting of an ensemble of absorbers all resonant at the same frequency, with equal populations, but with different dipole matrix elements. Essentially, the weaker transition elements contribute less to the absorption and are also more difficult to saturate. The first order effect is to produce an averaging in which the mean saturation intensity is somewhat greater than its value for the strongest matrix element components.

3.1.5 Bandwidth

For radiative transitions, the bandwidth of response to an applied field is given by the homogeneous width $\Delta\nu_h$. This width is related to T_2 through

$$B = \Delta\nu_h = \frac{1}{\pi T_2} \quad . \tag{30}$$

As indicated, T_2 represents the sum of several factors including spontaneous emission. However, for the pressure range under consideration, $1/T_2$ is primarily determined by the collision rate and as a result is proportional to $PT^{-1/2}$.

3.1.6 Dependence of Figure-of-Merit on Pressure and Temperature in Molecular Absorbers

The dependence of the quantity $(\alpha_o B/I_s)$ on pressure and temperature can be found in terms of the component parameters. Since α_o and B are both linear in pressure while I_s is quadratic, the net result is independent of pressure. The dependence on temperature is somewhat more complex. As has been shown in Section 3.1.2, for the special case of a low J transition and heavy spherical top molecule the absorption coefficient is proportional to T^{-3}. When the temperature dependence of B and I_s is included through the dependence of the collision rate, one finds that the figure-of-merit, F_M, is proportional to $T^{-5/2}$. For the linear molecule with low J number the result is proportional to T^{-2}.

3.1.7 Hole Burning and the Lamb Dip

The relationship between the saturated BALAD filter bandwidth and the homogeneous width can be understood with the phenomenological concept of "hole burning." The phenomenon of "hole burning" is fundamental to the operation of the BALAD receiver. The effect is used to produce the dynamic spatial, and temporal filter for the incident radiation.

Qualitatively, "hole burning" can be described in the following way: If a monochromatic field is applied to an inhomogeneously broadened absorber (Doppler broadened) at a frequency somewhat different from the resonant frequency, only a small group of molecules will absorb energy from the field; namely, those molecules that have the center of their response functions Doppler shifted to coincide with the field frequency. The width of the response to the field is determined by the homogeneous width of the optical transition, which in a gas is usually determined by a combination of radiative decay rates and collision rates. With sufficiently large field intensity, the number of absorbing molecules are depleted and the absorption becomes saturated or bleached. However, the saturation is limited to the particular velocity group that is resonant with the field. This localized saturation produces a "hole" in the equilibrium absorption frequency distribution. The width of the "hole" is comparable to the homogeneous line width. Since the saturation only appears in the region of strong field, the "hole" occupies the same cross-section as the strong field and therefore provides spatial filtering of the spontaneous emission from the preamplifier.

Hole burning can also be used to describe the "Lamb dip," an effect that is used experimentally in this program to obtain information about the location of the central frequencies of the saturable absorbers investigated and their homogeneous widths. If one considers, in addition to the strong monochromatic field, a second optical field at the same frequency travelling in the reverse direction to form a quasi-standing wave (the amplitudes of the two fields need not be equal), then two holes will be burned in the Doppler distribution. Although both fields are at the same frequency, the reversal of the direction changes the Doppler shift associated with the moving molecules in the laboratory frame and the oppositely directed fields interact with separate velocity groups. If the field frequency is tuned to resonance, only one group of molecules interacts with both fields (the zero velocity group) and the two holes coalesce into one. This results in an increase in the saturation of the absorbers and a consequent increase in the power transmitted through the medium. Because the hole widths are characteristic of the homogeneous width of the medium which may be as small as one percent of the Doppler width, the peak in the power output as a function of frequency determines a precise location of the line center.

3.1.8 Table of Molecular Absorbers

We have prepared a table of potential molecular absorbers for the CO_2 $00^{\circ}1 \rightarrow 02^{\circ}0$ and $00^{\circ}1 \rightarrow 10^{\circ}0$ transitions, that indicates the central frequency of the molecular vibrational band, its molecular weight (MW), sources of information and relevant known properties. Table 1 was prepared by utilizing standard reference texts such as "Infrared and Raman Spectra of Molecules," G. Herzberg; "Infrared Band Handbook," H. A. Szymanski; "N. B. S. Tables of Molecular Vibrational Frequencies;" and by a literature search of technical journals for reports of observed absorption coincidences between molecular transitions and CO_2 laser transitions. In addition, several transitions in the 3μ region are included in the table.

The most important physical property is the overlap between the amplification bandwidth of the laser material and the absorption line of the filter. Except for the relatively few cases of observed overlap reported in technical journals, the quality of the available information is inadequate to guarantee an overlap between the absorber and one of the CO_2 transitions. The reason for this is that the band centers are known to an accuracy in most cases of only ± 1 cm^{-1} or about 30 GHz while the amplification bandwidth in CO_2 is about 50 MHz or 1/600 of the uncertainty in resonant frequency. As a result, such a table can only be considered as a guide, and measurements with a CO_2 laser must be relied on to determine the extent of overlap. In some cases the overlap may be improved through shifting the resonant frequency by the Stark effect. This is a possibility for molecules such as, NH_3 and CH_3F which have large permanent dipole moments. However, as indicated in Section 3.1, the improvement in overlap that may be obtained for these molecules would be negated by the small transition intensity in comparison to SF_6.

Table 1. Table of Molecular Absorbers

Compound	MW	Reference	Band Center	Relevant Properties	
SF_6	146	A, B, N, O	10.6μ	$\alpha_o \approx 1.3$ cm^{-1} Torr^{-1}	(N)
BCl_3	55	A, E, G	10.6μ	$\alpha_o \approx 0.02$ cm^{-1} Torr^{-1}	(E)
H_2CO	30	A, O, P	10.6μ 9.6μ 3.5μ	Strong transition, $\alpha_o \approx 0.1$ cm^{-1} Torr^{-1}	(O) (P)
C_2H_3Cl	63	A, I	9.6μ	Q switched 9.2μ	(I)
NH_3	17	A, B, M, O	10.6μ	$\alpha_o \approx 1.6$ cm^{-1} Torr^{-1} (P(15) of N_2O) $\alpha_o \approx 3.6$ cm^{-1} Torr^{-1} (R(42) of CO_2)	
C_2H_4	28	A, B, C, L, O	10.6μ	Q switched P(16) and P(20) of CO_2 laser	
SiH_3Cl	67	A, O	10.6μ	-	
SiH_3Br	111	O	10.6μ	Strong transition	(O)
SiH_3I	133	A		-	
F_2O	54	A, O	10.6μ	Strong transition	(O)
PH_3	34	A		-	
C_3H_6	42	A, H, O, I	10.6μ 9.6μ	Q switched 10.6 Q switched 9.2	(H) (I)
D_2CO_2	48	A, H	9.6μ	-	
PF_5	127	B, J	10.6μ	$\alpha_o \approx 0.13$ cm^{-1} Torr^{-1}	(J)
CF_2Cl_2	121	B, F	10.6μ	$\alpha_o \approx 0.076$ cm^{-1} Torr^{-1}	(F)
D_2S	36	C	10.6μ	-	
$C_2H_2Cl_2$	97	C	10.6μ	-	
C_2H_6O	46	C	10.6μ	-	
C_6D_6	84	C	10.6μ	-	
$C_3H_6O_3$	90	D	10.6μ	Very strong (Q branch)	

Table 1. Table of Molecular Absorbers (Cont'd.)

Compound	MW	Reference	Band Center	Relevant Properties
C_6H_{14}	86	D	10.6μ	Very strong
C_2H_5Cl	65	D,O	10.6μ	Very strong
C_3H_2O	54	D	10.6μ	Very strong
$C_2F_4Cl_2$	172	D	10.6μ	Strong
$C_2H_4F_2$	66	D	10.6μ	Very strong
$C_2H_3Cl_3$	135	D	10.6μ	Medium strong
$C_2H_3Cl_2$	100	D	10.6μ	-
$H_2C_3N_2$	66	D,O	10.6μ	-
C_3H_4O	56	D	10.6μ	-
$C_2H_6SO_2$	94	D	9.6μ	-
C_3H_3I	166	D	9.6μ	-
C_3H_3Br	119	D	9.6μ	Very strong
C_2H_2FCl	80	D	9.6μ	-
SiF_4	105	D,O,Q	9.6μ	$\alpha_o \approx 0.334$ cm^{-1} Torr^{-1} (in present report)
C_2H_2BrF	125	D	9.6μ	-
C_4H_6	54	D	9.6μ	
C_3F_8	188	D	9.6μ	Medium strong
C_5H_{12}	72	D	9.6μ	Very strong
C_2F_3Cl	117	F,I	10.6μ 9.6μ	Q switched P(6) - P(20) of 9.6μ transition
CH_3F	34	J,O	9.6μ	Q switched; $\alpha_o \approx 0.3$ cm^{-1} Torr^{-1} if pure $^{13}CH_3F$ were used. (J)
C_2H_6O	46	K,O	3.5μ 10.6μ	$\alpha \approx 0.01$ cm^{-1} Torr^{-1} (K) Strong (O)

Table 1. Table of Molecular Absorbers (Cont'd.)

Compound	MW	Reference	Band Center	Relevant Properties
CH_3OH	32	L, O	9.6μ	Q switched
COD_xH_{4-x}	33-36	O	9.6μ	Weak to very strong (subscript x = 1, 2, 3, 4)
CD_3Cl	53	O	9.6μ	Strong
$C_2F_2Cl_2$	134	O	9.6μ	Very strong
H_2CO_2	46	O, H	9.6μ	Q switched 9.2μ (H)
C_2HF_2D	66	O	9.6μ	Very strong
H_2Se	81	O	9.6μ	Strong
C_6H_{12}	84	O	9.6μ	Medium strength transition
CH_5N	32	O	9.6μ	Strong
C_4D_8	64	O	9.6μ	Strong
C_2H_5F	48	O	9.6μ	Very strong
C_3H_8	44	O	9.6μ	Medium
$C_2H_3O_2D$	61	O	9.6μ	Weak
HC_2F	44	O	9.6μ	Very strong
CD_3Cl	54	O	9.6μ	Medium
C_2H_5Br	110	O	9.6μ	Very weak
CD_3NH_2	33	O	9.6μ	Weak
GeH_4	77	O	10.6μ	-
C_3H_4	40	O	10.6μ	Weak (will explode from mechanical shock)
CD_5N	35	O	10.6μ	Strong
SiH_2D_2	34	O	10.6μ	Weak

Table 1. Table of Molecular Absorbers (Cont'd.)

Compound	MW	Reference	Band Center	Relevant Properties
CH_3NC	41	O	10.6μ	Medium (will explode from mechanical shock)
CD_3I	145	O, A	10.6μ	-
SiH_3F	50	O	10.6μ	Medium
$^{11}B_2H_6$	28	O	10.6μ	Strong (can react explosively with oxides)
$^{10}B_2H_6$	26	O	10.6μ	Strong (can react explosively with oxides)
CH_4	16	P	3.39μ	$\alpha_o \approx 0.17$ cm^{-1} Torr^{-1}
H_2CO	30	P	3.5μ	$\alpha_o \approx 0.1$ cm^{-1} Torr^{-1}
CH_3Br	95	O	10.6μ	Medium strength
$CD_2C\ell Br$	131	O	10.6μ	Strong
NF_3	71	O	9.6μ	Strong (will explode from mechanical shock)
CH_xCOD_{6-x}	49, 52	O	9.6μ	Strong (subscript x = 0, 3)
C_2D_4O	48	O	10.6μ	Very strong
CHFCDF	65	O	9.6μ	Very strong

References for Table of Molecular Absorbers

A BALAD Contract Proposal, April 1970.

B Christian Borde, C.R. Acad. Sc. Paris, t. 270 (1970).

C "Infrared and Raman Spectra," G. Herzberg, Princeton, New Jersey, D. Van Nostrand Co., Inc., 1955.

D "Infrared Band Handbook," H. A. Szymanski (editor), 1963, Plenum Press, New York.

E John H. McCoy, Appl. Phys. Lett. 15, 353 (1969).

F S. Marcus, Appl. Phys. Lett. 15, 217 (1969).

G Karlov, et al., JETP Lett. 7, 134 (1968).

H Hanst, et al., Appl Phys. Lett. 12, 58 (1968).

References for Table of Molecular Absorbers (Cont'd.)

I Day, et al., Proc. IEEE (letters), 57, 2060 (1969).

J Chang, Wang, and Cheo, Appl. Phys. Lett. 15, 157 (1969).

K Wang, et al., J. Quan. Electr. QE-6, 576 (1970).

L Jensen and Tobin, J. Quan. Electr. QE-6, 477 (1970).

M Shimizu, Appl. Phys. Lett. 16, 368 (1970).

N Paul Rabinowitz, P.I.B. Technical Report (PIBEP-70-065).

O N.B.S. Tables of Molecular Vibration Frequencies, NSRDS NBS-6, 11, 17.

P V.S. Letokhov, Soviet Physics, JETP, 7, 88 (1968).

Q Jon Hall, J.I.L.A. (private communication).

3.2 Experimental Investigation of Molecular Absorbers

From the data available in the literature, no clear cut selection can be made among the various molecules on the list. The primary reason for this is the uncertainty in the resonant frequencies. Although, one would like to remove from the list heavy molecules with large moments of inertia for example, on the basis that the strength and bandwidth of absorption resonances associated with such molecules would not be as suitable as those from lighter molecules, one cannot because, as in the case of SF_6, one may find that the overlap more than makes up for the other factors.

As a result, we considered processing, via the measurement procedure, as many potential absorbers as possible. Some materials are not readily available and were not considered. For example, many of the deuterated molecules cannot be obtained from standard chemical manufacturers, or as is often the case cannot be separated in pure form, the higher order deuterated and undeuterated forms being present as impurities. Many materials listed in the table are either highly reactive or explosive and were rejected on that basis.

3.2.1 Experimental Procedure

Because of the great uncertainty in the known values of resonance frequencies of potential molecular absorbers, a three step procedure of absorption measurements was instituted to examine various absorbers.

The procedure consisted of:

1. Single point attenuation measurements on all possible laser transitions falling within the absorption band of the molecule at pressures sufficiently high to preclude saturation; so that small signal absorption coefficients could be obtained.

2. If the results from step 1 indicated significant absorption on any transitions, measurements of attenuation as a function of absolute intensity and gas pressure were then made on each laser transition where overlaps were found. In this way, absorption coefficients and saturation intensities were determined as a function of pressure.

3. The absorption centers were located relative to the amplification bandwidth by Lamb dip measurements. The dependence of the dip width on pressure was used to determine the homogeneous width and phase interruption time T_2. In this way, the pertinent parameters α_o, I_s, and B for determining F_M were obtained.

3.2.2 Experimental Arrangement

The experimental arrangement for absorption measurements is shown in Fig. 7. The laser plasma tube (CO_2:N_2:He:Xe:H_2 = 2:4:8:2:0.1 Torr) is 90 cm long has an i. d. of 1 cm and is operated sealed off with an output of about 3 watts. The cavity is 1 meter long and operates in a folded confocal configuration. Transverse mode selection is achieved by constricting an iris aperture within the cavity. Wavelength selection is provided by a diffraction grating, blazed for 10μ, which is used as the plane reflector in the cavity. The sphere which is dielectric coated (96% reflectance) is mounted on a piezoelectric transducer to provide cavity tuning, which for this case, has a measured sensitivity of 0.10 MHz/volt. The output beam is brought to a focus and an iris aperture is used to spatially filter spurious reflections that would interfere with the main beam. The beam is passed through a 26 cm attenuation cell and then collimated before entering the absorption apparatus.

Two beam splitters are used to provide a separate reference beam with each beam being examined alternately. The primary beam is passed through the gas absorption cell (25 cm long) where the pressure is monitored by an MKS Baratron capacitance manometer. The beam is chopped and enters a Perkin-Elmer monochromator to determine the wavelength of the transition. Detection is with a Santa Barbara Research Center GE:Au Detector (407A). The output of the detector is displayed on an oscilloscope and examined by a Princeton Applied Research JB-5 lock-in amplifier. Absolute intensity measurements are made with an Epply thermopile that is placed in the position indicated in the figure. The measurements are normalized by comparing the primary to reference beam intensities with the absorption cell evacuated. In addition, the zeroth order output of the laser cavity grating is monitored with a CRL power meter and is peaked to maintain the oscillation at line center. The intensity of the primary beam is controlled by adjusting the vapor pressure of methanol in the attenuator cell.

With relatively small alterations, the same apparatus is used to observe Lamb dips. Mirror M3 is rotated so that the beam very nearly returns on itself to focus in

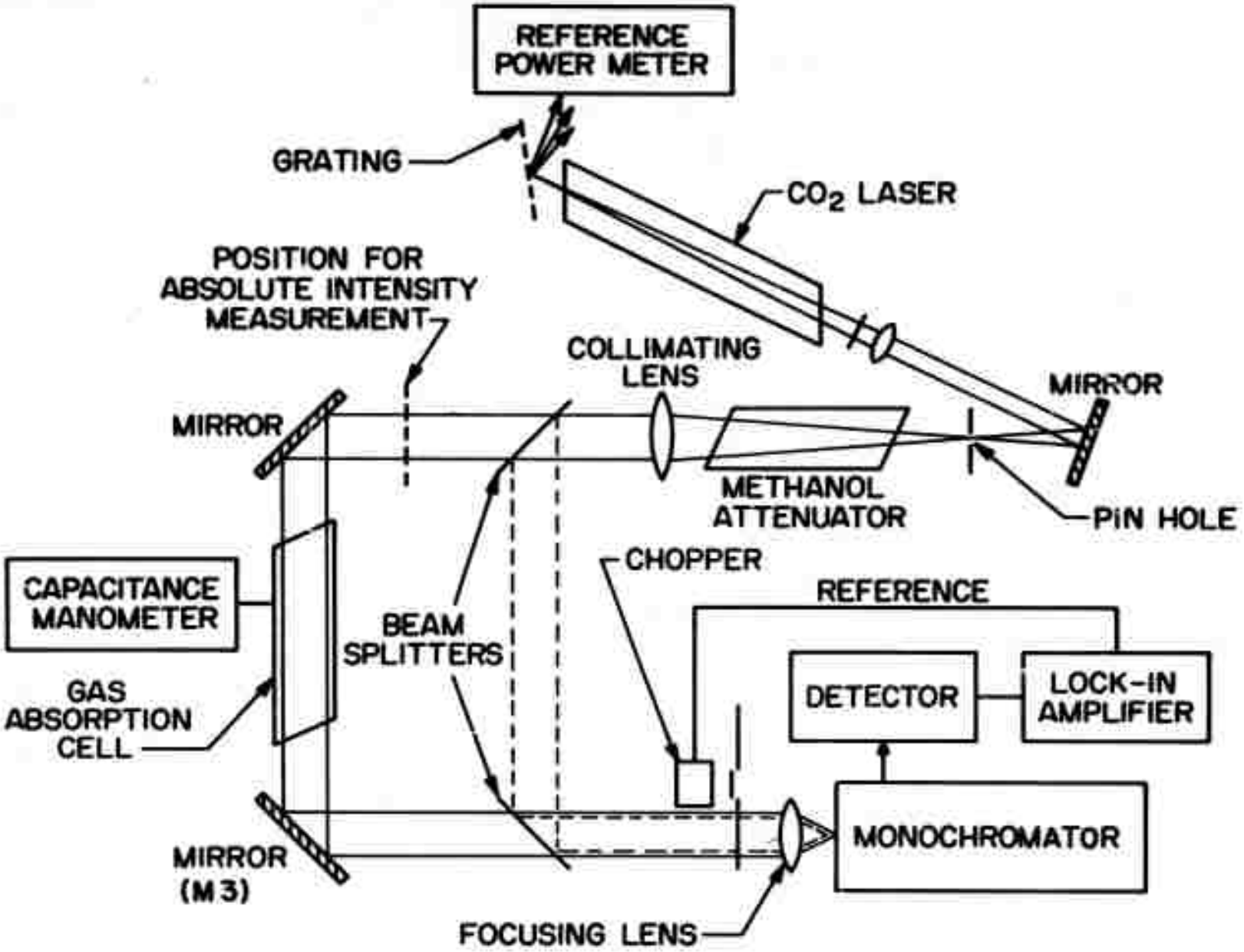

Fig. 7 - Apparatus for absorption measurements

the neighborhood of the pin hole. This approximately produces a standing wave in the absorption cell. The angular deviation between the forward and reverse beam is less than 10^{-2} radians. The return beam is picked off with a mirror near the pin hole and passed through the monochromator. After detection, the output is displayed on an oscilloscope while the frequency of the laser is swept by applying the saw-tooth voltage of the oscilloscope directly to the piezoelectric transducer. The reference arm and chopper are not employed in this measurement. The frequency width and relative locations of the dips are obtained from the display by utilizing the piezoelectric transducer calibration.

3.2.3 Experimental Results

The absorption properties of four gases: methanol CH_3OH, ethylfluoride C_2H_5F, silicon tetrafluoride SiF_4, and sulpherhexafluoride SF_6, each with strong absorption resonances near the CO_2 $(00^o1 \rightarrow 02^o0)$ or $(00^o1 \rightarrow 10^o0)$ band were investigated. The laser output for the P branch of the $(00^o1 \rightarrow 02^o0)$ band is shown in Fig. 8.

The first two gases were taken only through the first stage of the measurements. The results are shown in Figs. 9 and 10. The maximum absorption coefficient for methanol on the P(32) line of CO_2 is less than 0.33 cm^{-1} $Torr^{-1}$ and the maximum absorption coefficient for the ethylfluoride is less than 0.013 cm^{-1} $Torr^{-1}$ on the CO_2P(14) transition. In both cases the small values of absorption coefficient did not justify further examination.

A more complete set of measurements has been made on SiF_4, which we believed had absorption properties comparable to SF_6. SiF_4 is a spherical top molecule with the center of the ν_3 band at 1031.8 cm^{-1}, in the neighborhood of the P(36) line of the CO_2 laser. Absorption line center coincidences were found on six CO_2 lines from the P(26) to the P(36). These absorption centers which lie primarily in the R branch of the absorption band are shown in Fig. 11, the results of Lamb dip observations.

The absorption data was taken on the four strongest absorption lines, corresponding to the CO_2 P(28), P(30), P(32), and P(36) lines. A plot of attenuation as a function of intensity is shown in Fig. 12 for absorption on the P(30) at a pressure of 100m Torr. The extrapolated value of the attenuation to low intensities determines the absorption coefficient at this pressure. The absorption coefficients as a function of pressure for the four strongest lines, each point representing an extrapolation to zero intensity, is shown in Fig. 13.

One cannot directly measure the saturation intensity. For an infinite inhomogeneous line, the absorption coefficient saturates as function of intensity in the following way:

$$\alpha = \frac{1}{I} \cdot \frac{dI}{dz} \cong \frac{\alpha_o}{(1 + I/I_s)^{1/2}} \qquad (31)$$

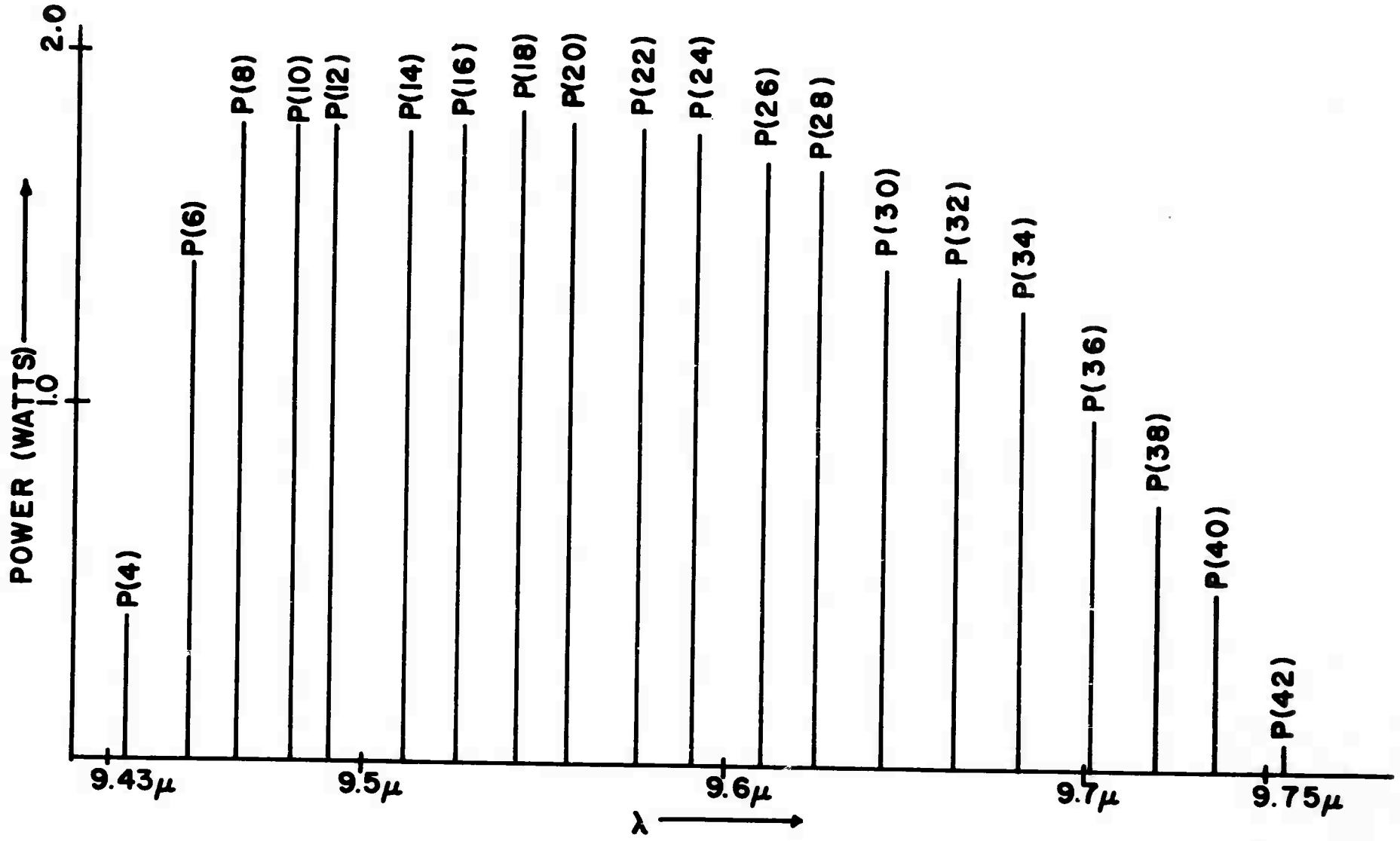

Fig. 8 - Oscillating lines of 9.6μ CO_2 laser

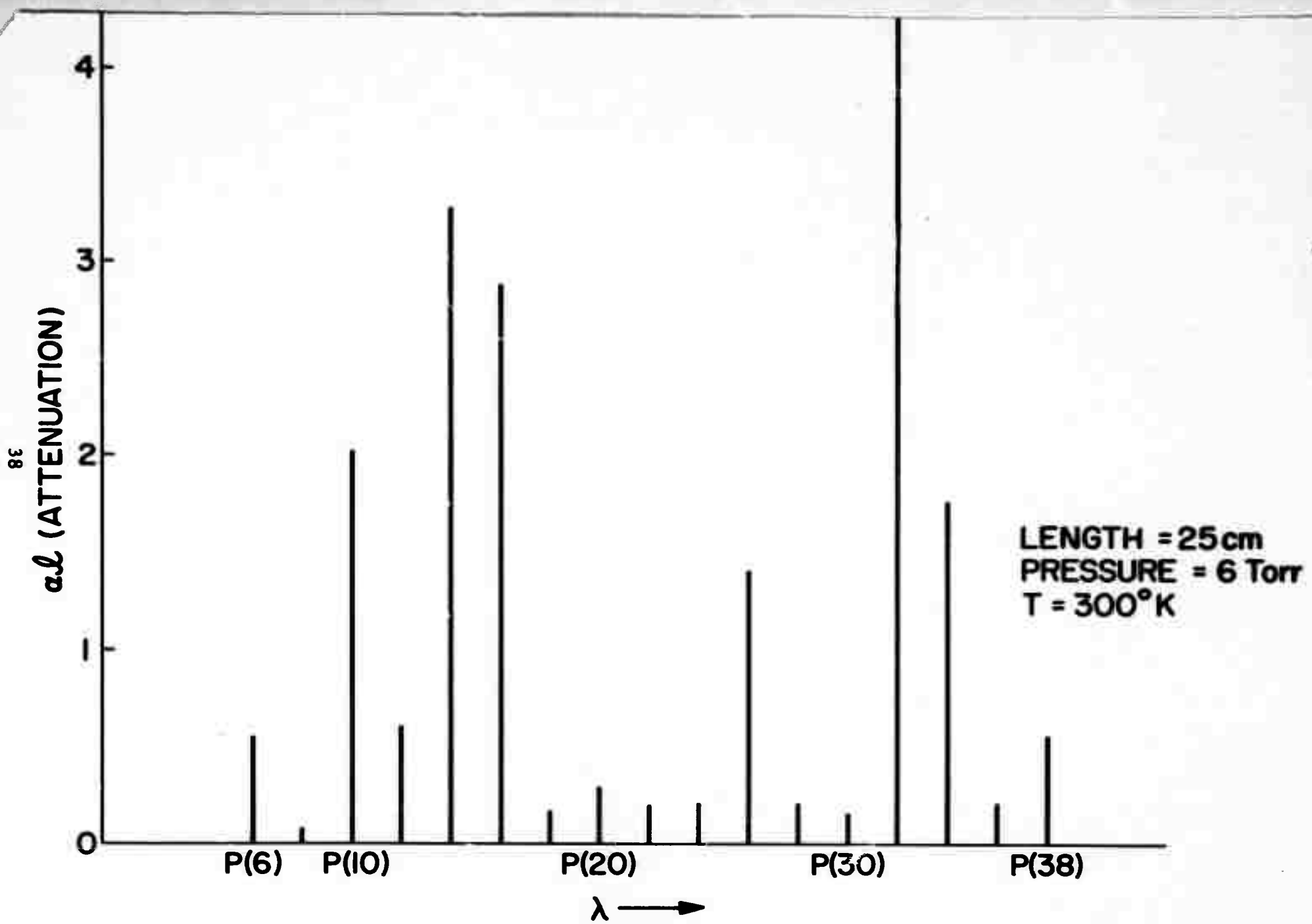

Fig. 9 - Unsaturated single pass absorption by methanol for lines of CO_2 ($00^0 1$-$02^0 0$) band

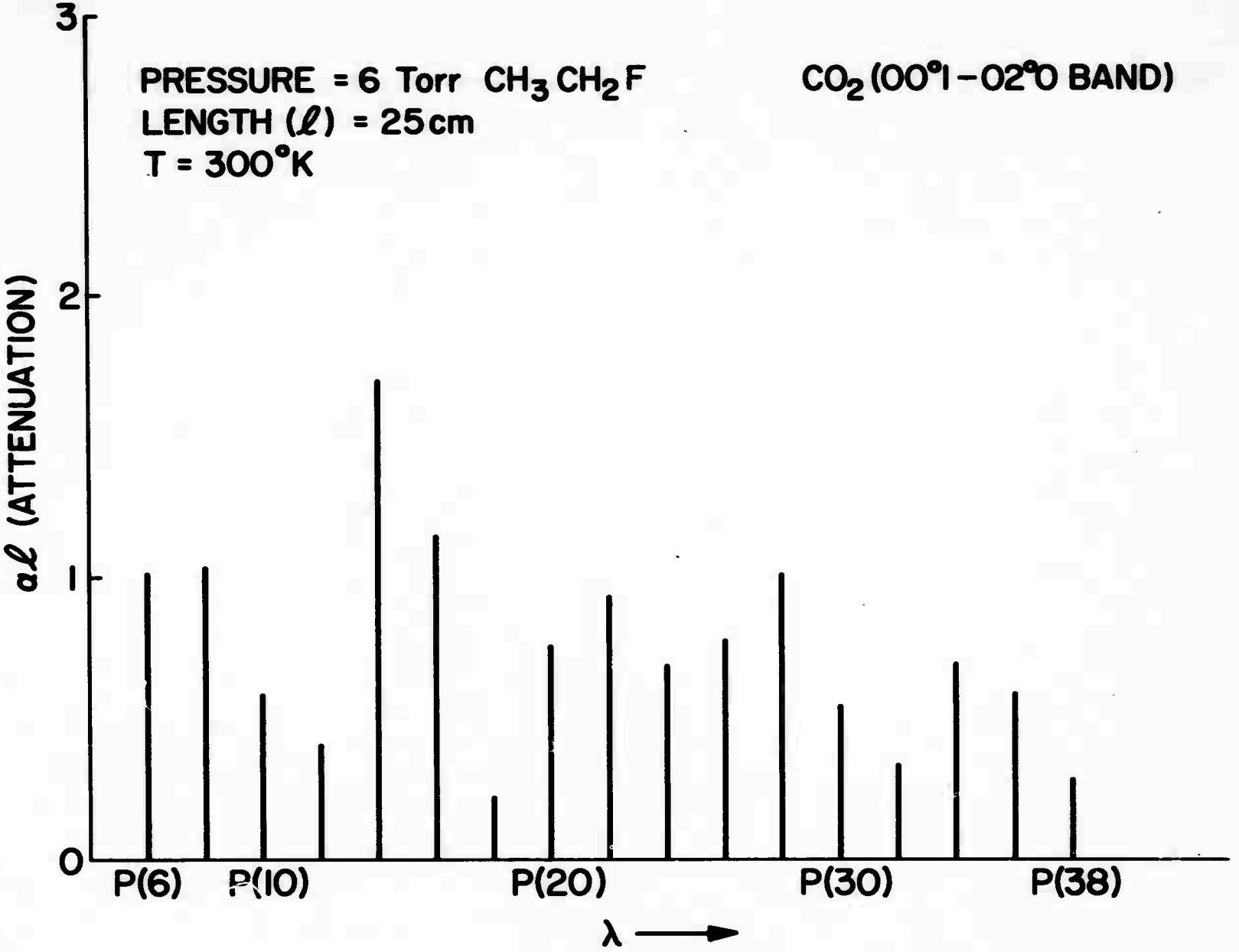

Fig. 10 - Unsaturated single pass absorption by ethyl fluoride

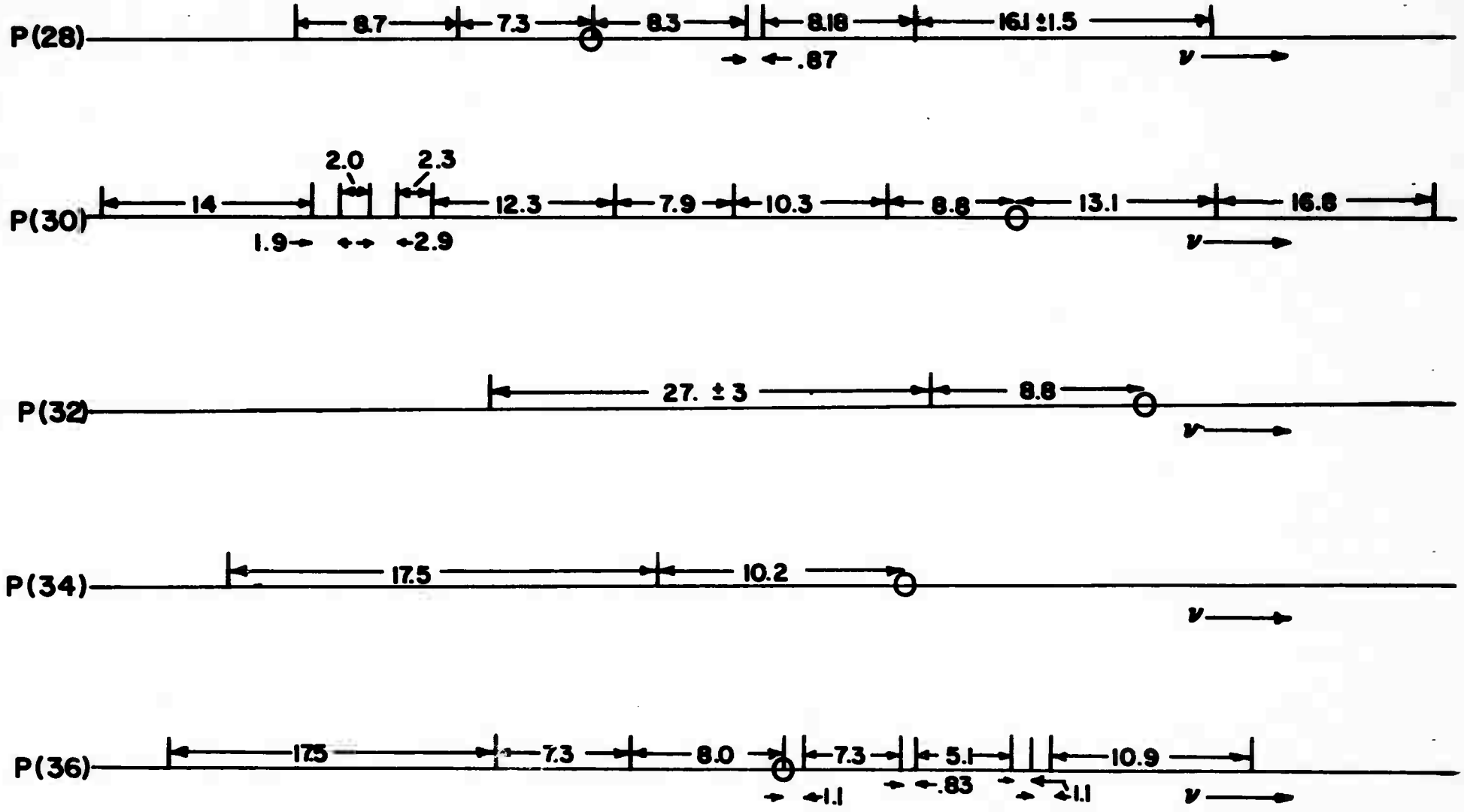

Fig. 11 - Lamb dip spectrum of SiF_4

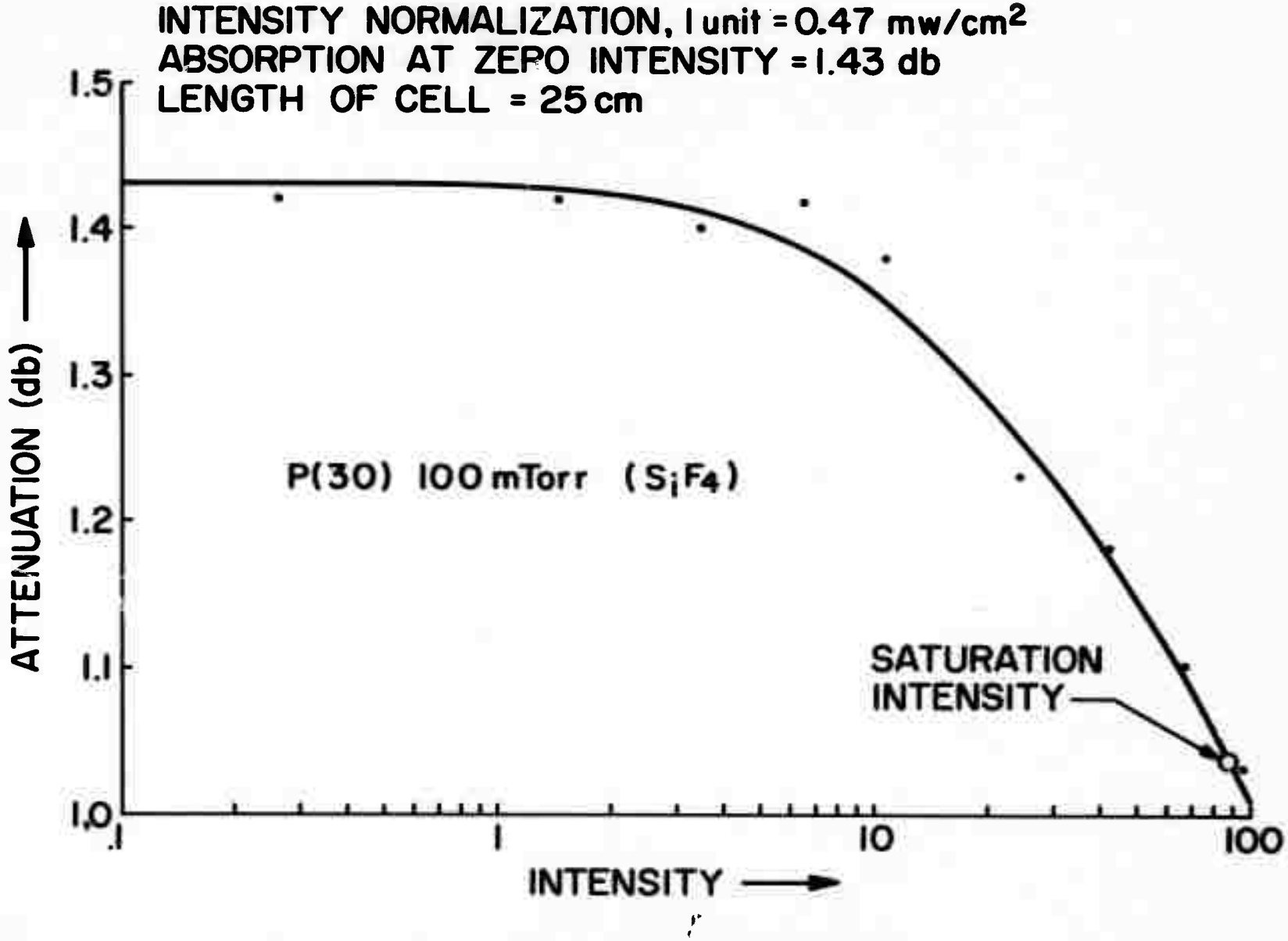

Fig. 12 - Attenuation vs. input intensity in SiF_4

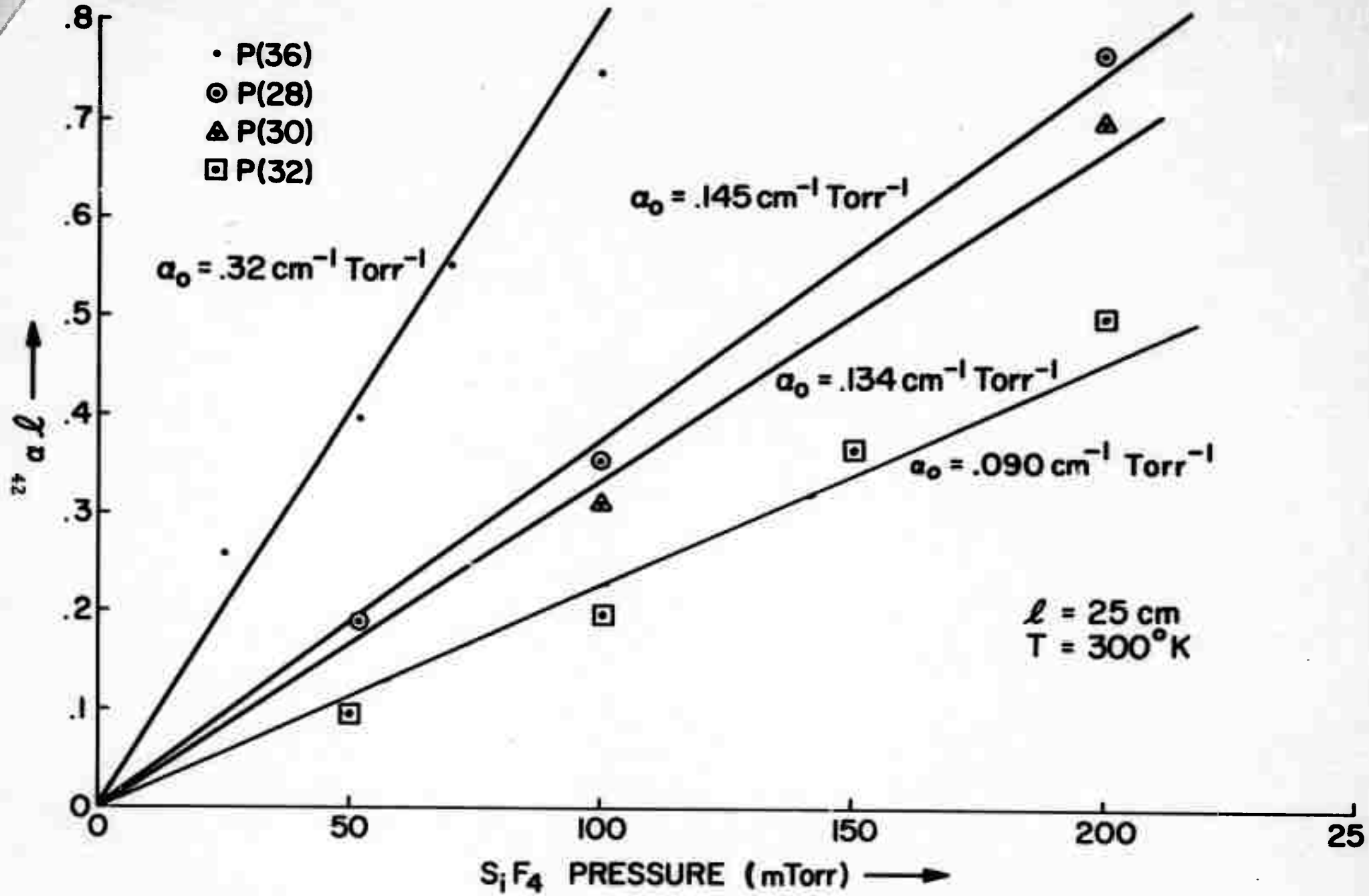

Fig. 13 - Small signal absorption vs. pressure of SiF_4

where I_s is the saturation intensity.

This equation can be integrated exactly to

$$-\alpha_o \ell = \left\{ 2(1+I/I_s)^{1/2} + \ell n \left[\frac{(1+I/I_s)^{1/2} - 1}{(1+I/I_s)^{1/2} + 1} \right] \right\} \Bigg|_{I(0)}^{I(\ell)} . \qquad (32)$$

This equation can also be corrected for a finite Doppler width to[16]

$$-\alpha_o \ell = \left\{ 2(1+I/I_s)^{1/2} + \ell n \left[\frac{(1+I/I_s)^{1/2} - 1}{(1+I/I_s)^{1/2} + 1} \right] + \frac{2\epsilon}{\pi \frac{1}{2}} [(I/I_s) + \ell n(I/I_s)] \right\} \Bigg|_{I(0)}^{I(\ell)} \qquad (33)$$

where $\epsilon = (\Delta\nu_h / \Delta\nu_d)(\ell n 2)^{1/2}$, and it is assumed that $\epsilon << 1$.

If the value of the absorption coefficient is obtained by extrapolation of the logarithm of attenuation to zero intensity, then this value can be substituted in Eq. (33) to find the value of the attenuation for $I = I_s$. In this way I_s may be obtained. A machine calculation of the attenuation for $I = I_s$, for two values of $\Delta\nu_h / \Delta\nu_d$, is shown in Fig. 14.

A plot of the pressure dependence of the saturation intensity is shown in Fig. 15. Within the pressure range examined, the dependence is approximately quadratic as has also been reported for SF_6.[15, 17] This result can be understood in terms of the dependence of T_1 and T_2, the population and phase relaxation times, on pressure which was discussed in Section 3.1.3.

The dependence of the homogeneous width on pressure can be found by examining the Lamb dip width as a function of pressure. This was done by monitoring the width of the central dip on the P(28) line at different pressures while lowering the intensity to a level at which power broadening was not observed. The results are shown in Fig. 16. An interesting result is that the plot does not pass through zero width at zero pressure. The intercept at about 400 kHz is too large to be explained by spontaneous emission or time of flight effects due to finite beam width which at most would produce an effect of about 10 kHz. We believe that the effect is mainly instrumental, due to misalignment between the forward and reverse beam and probably also to microphonic spread of the frequency spectrum of the laser.

For small saturation intensities the Lamb dip width in an external absorption cell is equal to the homogeneous width

$$\Delta\nu_{\text{Lamb dip}} = \Delta\nu_h . \qquad (34)$$

The data shown in Fig. 16 indicates the rate of increase of homogeneous width with pressure is 6.05 MHz/Torr which corresponds to a value of T_2 of 5×10^{-8} Torr-sec.

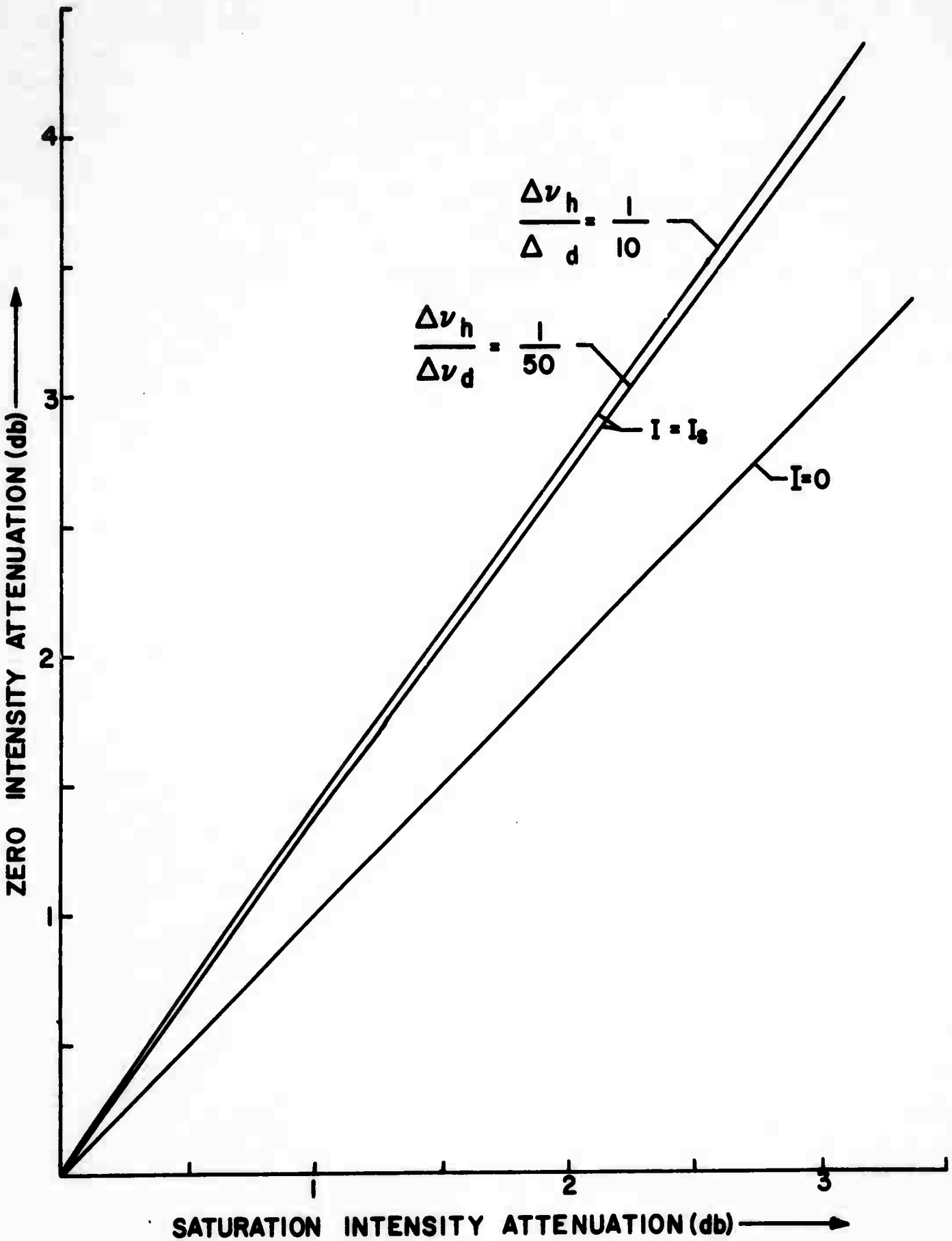

Fig. 14 - Attenuation at zero vs. attenuation at saturation intensity

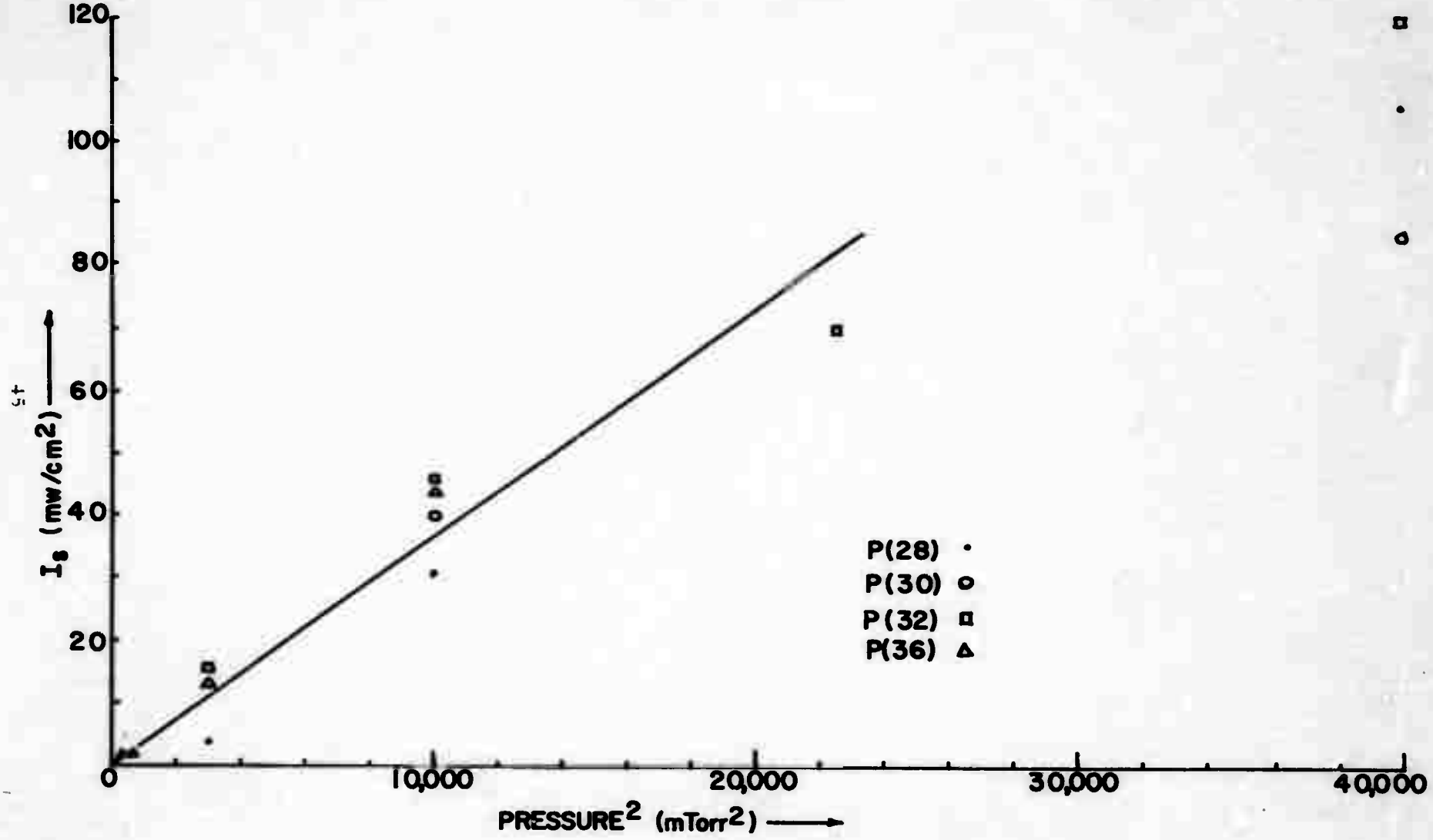

Fig. 15 - Saturation intensity vs. pressure-squared of SiF_4

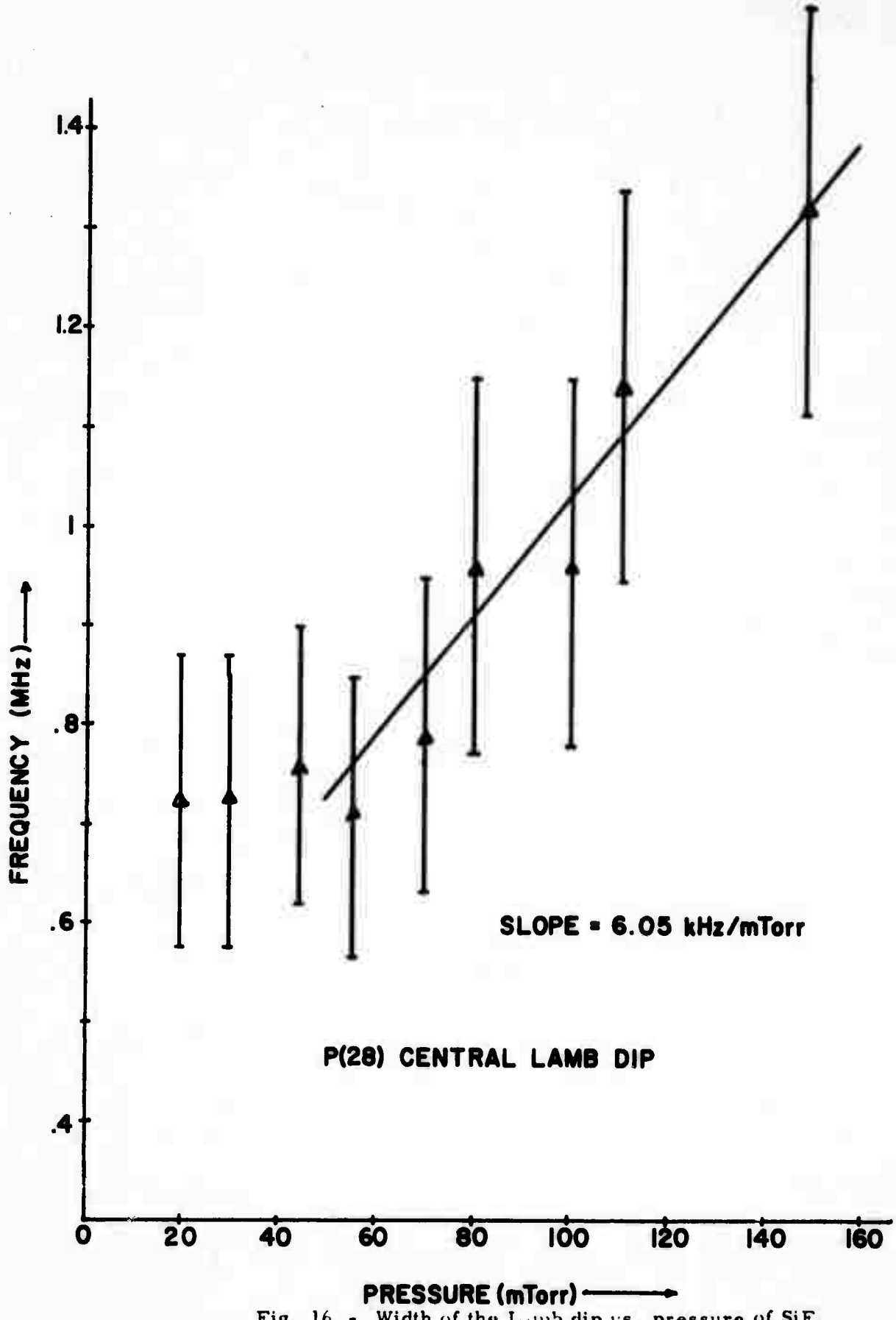

Fig. 16 - Width of the Lamb dip vs. pressure of SiF_4

3.2.4 Measurement of Temperature Dependence of SF_6 Absorption

In Section 3.1.2, it was shown that a substantial increase in F_M is obtainable by reducing the temperature of a heavy spherical rotor, SF_6, e.g. However, a minimal vapor pressure at the reduced temperature is required, to utilize the increase in absorption coefficient that accompanies the reduction of temperature. Because SF_6 does not have an adequate vapor pressure at liquid nitrogen temperatures (78°K) to produce any measurable absorption, the question arises as to what is the lowest working temperature that can be utilized with SF_6. We have extrapolated vapor pressure data[18] using the following expansion for the vapor pressure

$$\log P = A_1 + \frac{A_2}{T} + A_3 \log T \quad , \tag{35}$$

to obtain the curve shown in Fig. 17. The results of the extrapolation indicate that operation at temperatures as low as 120°K are possible, with an increase in absorption by a factor of 15.

For the measurement of the temperature dependence of SF_6 absorption an apparatus similar to that shown in Fig. 7 was used. The SF_6 pressure was maintained at 30m Torr. The absorption cell which was 54.5 cm long had an outer jacket which could be filled with a mixture of acetone and dry ice. The measurements on the P(16) line of CO_2 consisted of finding the transmission as a function of input intensity at temperatures of 25°C and -60°C. The ratio of the extrapolated value of the zero field absorption was found to be 2.35. This should be compared with a calculated ratio of 2.74, which assumes an inverse cubic dependence on temperature. The discrepancy which is small, is probably due to the thermal gradients in the absorption cell, and the approximate nature of the calculated expression which rounds off the exponential term in the temperature dependence (see Section 3.1.2).

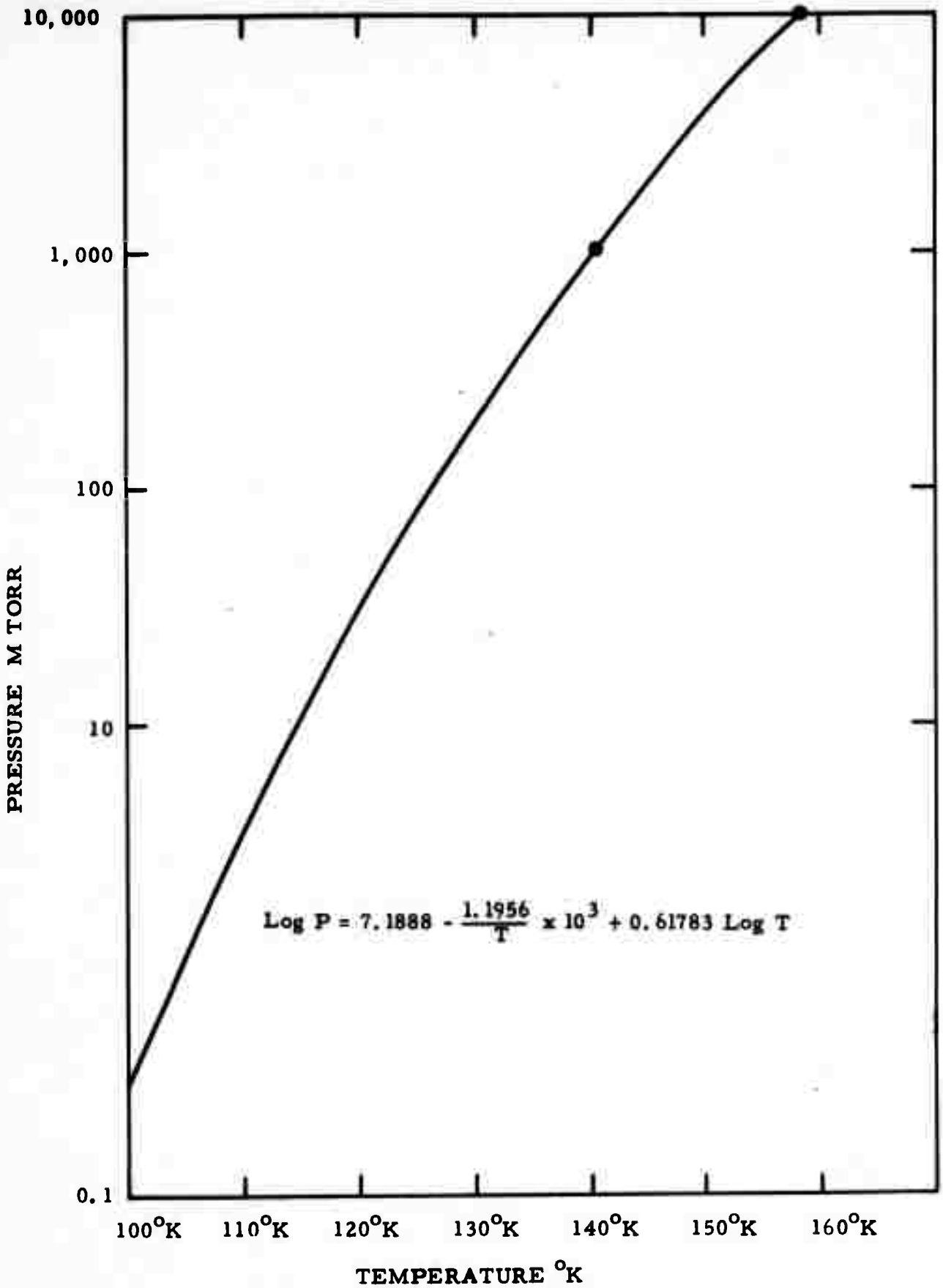

Fig. 17 Extrapolated SF_6 vapor pressure vs. temperature

4.0 EXCITED ATOMIC ABSORBERS

An atomic absorber with a resonance line (i.e., a ground state transition) which coincides with a suitable laser transition would make an ideal absorber for a BALAD receiver. As discussed in Section 3, an allowed electric dipole transition would yield the large absorption coefficient and small saturation intensity as desired. Also, an atom lacks rotational and vibrational degrees of freedom, and has no low dying energy levels which insures that all atoms would be in the ground state and contribute to the resonance line absorption. Unfortunately, no such coincidence has been discovered, and it is unlikely that any exist.

The next area to explore would be absorption lines from low lying energy levels of atoms. Since, as just mentioned, few atoms have energy levels which can be thermally populated at reasonable temperatures (all atomic energies >> kT) this implies the need of an electrical discharge to populate even low lying atomic levels. Also, most absorption lines from low lying levels (including the ground state) fall in the visible or ultraviolet portion of the spectrum. Therefore, if a chance coincidence were found, it would most likely be a short wavelength laser system. Unfortunately, infrared absorption (and emission) lines usually terminate in higher lying energy levels, which would require a substantial level of electrical discharge excitation to produce the needed lower level population.

The obvious exception to the poor chance of finding a coincidence between a laser and an absorber is to consider the active medium of the laser itself as an absorber. In this case, obviously, the "overlap" between the laser and absorber would be exact and complete, unless the operating conditions were so different that there was a significant frequency shift in either the laser or absorber.

Various laser media were considered for possible use as absorbers, including molecular lasers such as CO_2 and self terminating lasers such as N_2, Ne, and Cu.

On the surface, CO_2 appears attractive because its low lying energy levels can even be thermally populated. Unfortunately, the statistical weight of the rotational degree of freedom is overwhelming. If one thermally populates the (lower laser) vibrational level, one also succeeds in populating such a large number of rotational levels that a high pressure is required to achieve a significant absorption coefficient. But then one loses the advantage of the spectral filter part of the BALAD, since the homogeneous width becomes pressure broadened and finally, the saturation intensity increases significantly. Overall, the figure-of-merit, F_M, decreases drastically, and so the attempt to use CO_2 as an absorber was abandoned in favor of SF_6 at 10.7μ.

The case of the self terminating lasers has not been considered in detail. The obvious drawback is the limited time duration over which gain persists. Since the self

terminating laser amplifier operates only in a pulsed mode, the excitation of the amplifier would have to be synchronized to coincide with the arrival of the signal.

Of the various cw lasers, the He-Xe laser appears to be the most attractive for a BALAD receiver.

4.1 The Theory of the Excited Xenon Absorber

There have not been many reports in the literature on xenon and He-Xe lasers.[19, 20, 21] The most extensive study was found in a technical report.[22] The present work has extended the range of operation of the xenon laser in order to achieve absorption.

The first order theory of the operation of a ("4-level") laser medium generally assumes the electron energy distribution is a Boltzmann distribution at a temperature, T_e, and considers the amount of excitation of any level to be small, compared to the equilibrium (Boltzmann factor) population at the electron temperature. That is, the energy distribution of electrons is

$$n_e(E) = N_e \exp(-E/kT_e)(4E/\pi k^3 T_e^3)^{1/2} \tag{36}$$

and the population n_i of any atomic energy level E_i, satisfies

$$n_i << n_o \exp(-E_i/kT_e) \tag{37}$$

where n_o is the ground state population density ($E = 0$).

As a result, the first order rate equation for the population n_3 of the upper laser level (at energy E_3) is described by

$$\frac{d}{dt} n_3 = r_3 - n_3/t_3 \tag{38}$$

where $r_3 = n_o n_e \langle \sigma_{3o} v \rangle$ is the rate of excitation by electrons from the ground state, which is proportional to the product of n_o and the total electron density n_e and depends on the excitation cross section σ_{3o} and electron velocity v. The sharp brackets denote an average over the electron energy distribution. The upper state lifetime t_3 is usually dominated by spontaneous emission to various lower lying levels, but could include collisional de-excitation.

In steady state ($dn_3/dt = 0$), the solution is

$$n_3 = r_3 t_3 = n_e[n_o \langle \sigma_{3o} v \rangle t_3] \quad . \tag{39}$$

The lower state population n_2 is governed by a similar rate equation, except that the rate of direct excitation from the ground state is usually small, so that, two stage excitation via another level is generally dominant, and one can easily include a number of other levels which might contribute, giving

$$r_2 = n_e n_o \langle \sigma_{2o} v \rangle + \sum_i n_e n_i \langle \sigma_{2i} v \rangle \quad . \tag{40}$$

Introducing the steady state populations for n_i (similar to Eq. 39), we find

$$n_2 = n_e [n_o \langle \sigma_{2o} v \rangle t_2] + n_e^2 [\sum_i n_o \langle \sigma_{2i} v \rangle \langle \sigma_{io} v \rangle t_i t_2] \tag{41}$$

when $n_e n_i \langle \sigma_{2i} v \rangle << (1/\tau_i)$. Since the square brackets in Eqs. (39) and (41) contain only constants (to first order), and the current I in a discharge is proportional to the electron density

$$I = n_e [\mu E \cdot A] \quad , \tag{42}$$

the expressions for n_3 and n_2 can be written

$$n_3 = K_3 I$$

$$n_2 = K_1 I + K_2 I^2 \tag{43}$$

and the laser gain coefficient can be written

$$\alpha = \left[\frac{\lambda^2 \cdot A_{32}}{8\pi \Delta\nu}\right] (n_3 - n_2) \quad , \tag{44}$$

so

$$\alpha(I) = C_1 I - C_2 I^2$$

$$= C_1 I [1 - (I/2I_M)] \tag{45}$$

where $I_M = (C_1/2C_2)$ is the current for maximum gain. Indeed, the gain coefficient of many gas lasers have been observed to follow such a parabolic dependence on current.[23] From this model, one can see clearly that the transition from optimum conditions for gain to optimum conditions for absorption is simply a matter of increasing the current! In fact, for $I = 2I_M$, $\alpha(2I_M) = 0$ (the medium is transparent) and for $I = 4I_M$, $\alpha(4I_M) = -4C_1 I_M = -8\alpha_M$. Thus, on the basis of this model, it would seem one can easily produce an absorber with ten times the negative of the maximum gain coefficient. However, the model also predicts that an infinite absorption coefficient can be produced, whereas we know the maximum population of the level is limited by the Boltzmann factor and the finite ground state population.

The necessary correction to the model, which will insure the latter limit, is to include electron de-excitation of the atomic levels. Although this can be implicitly

included as a modification of the level lifetime, it is preferable to explicitly state the net rate of electron excitation so that Eq. (38) becomes:

$$\frac{dn_3}{dt} = n_e n_o \langle \sigma_{3o} v \rangle - n_e n_3 \langle \sigma_{o3} v \rangle - \frac{n_3}{\tau_3} \tag{46}$$

where σ_{o3} is the cross section for electron de-excitation. From detailed balancing, one can easily show the energy dependence of the excitation and de-excitation cross-sections are related by

$$\sigma_{3o}(E) = \frac{E - E_3}{E} \sigma_{o3}(E - E_3) \quad . \tag{47}$$

Using this result, the two averages over the (Boltzmann) electron energy distribution can be related

$$\langle \sigma_{3o} v \rangle = \exp(-E_3/kT_e) \langle \sigma_{o3} v \rangle \quad . \tag{48}$$

As a result, the steady state solution to Eq. (46) can be expressed

$$n_3 = \frac{n_o \exp(-E_3/kT_e)}{1 + \frac{1}{\tau_3 n_e \langle \sigma_{o3} v \rangle}} \quad . \tag{49}$$

This, of course, reduces to Eq. (39) when $1/t_3 >> n_e \langle \sigma_{o3} v \rangle$, i.e., when radiative decay dominates electron de-excitation.

If the similar net rate of electron excitation included for all level populations steady state solution for n_2 is:

$$n_2 = \frac{n_e n_o \langle \sigma_{2o} v \rangle + n_e \sum_i n_i \langle \sigma_{2i} v \rangle}{\frac{1}{\tau_2} + n_e \langle \sigma_{o2} v \rangle + n_e \sum_i \langle \sigma_{i2} v \rangle} \tag{50}$$

or

$$n_2 = \frac{n_o \exp(-E_2/kT_e) \left[n_e \langle \sigma_{o2} v \rangle + n_e \sum_i \langle \sigma_{i2} v \rangle \left(1 + \frac{1}{\tau_i n_e \langle \sigma_{o2} v \rangle} \right)^{-1} \right]}{\frac{1}{\tau_2} + n_e \langle \sigma_{o2} v \rangle + n_e \sum_i \langle \sigma_{i2} v \rangle} \quad . \tag{51}$$

This result similarly reduces to Eq. (41) for

$$\frac{1}{\tau_i} >> n_e \langle \sigma_{oi} v \rangle \qquad \text{and} \qquad \frac{1}{\tau_2} >> n_e \langle \sigma_{o2} v \rangle + \sum_i \langle \sigma_{i2} v \rangle$$

i.e., when all radiative decay rates dominate all electron de-excitation processes. Both Eqs. (51) and (49) clearly illustrate that n_2 and n_3 are limited to their Boltzmann factor population.

The actual electron energy distribution in a laser type gaseous discharge generally has a "depleted tail." That is, the number of high energy electrons is less than one would predict on the basis of a Boltzmann distribution, if one uses the temperature obtained from the low energy end of the electron distribution. Since the low energy electrons (which de-excite) are plentiful, the depletion of the high energy electrons implies that the maximum atomic level populations will be reduced. Although a quantitative statement would have to be based on a precision measurement of the electron energy distribution, the result can probably be approximated by using a somewhat lower excitation temperature to describe the maximum atomic energy level populations.

The precise behavior of a gaseous laser medium as a function of discharge current depends sensitively on radiation trapping which can greatly increase the lifetime of states which decay to the ground state. Indeed, it is the existence of radiation trapping which makes possible gas discharge excitation of lasers. Otherwise the spontaneous decay back to the ground state would make it very difficult to build up the required population in the upper laser level.

We must remember that large electron excitation cross section and large spontaneous emission transition probabilities go together, since they both depend on the same electric dipole matrix elements.

The energy level structure of xenon is indicated in Fig. 18. As indicated by the dashed lines, there are large electron excitation cross sections from the ground state to all of the s and d levels, and very little direct electron excitation of the p levels. The 3.507μ laser emission arises from the transition $5d[7/2]_3 \rightarrow 6p[5/2]_2$ as indicated. The population of selected levels among the 5d, 6p, and 6s levels were studied as a function of current in Ref. 25. They observed a quadratic growth of the 6p levels, and they observed the saturation of populations in the 5d and 6s levels. Since the object of that study was the optimization of the xenon laser, the study did not extend into the range of absorption.

4.2 Experimental Investigation of the Excited Xenon Absorbers

4.2.1 Gain and Absorption Measurements

The experimental apparatus and procedure for the gain measurements on xenon are very similar to the absorption measurements made on SiF_4 as discussed in Section 3.2. The laser was operated in a single transverse mode. The attenuation of the beam was accomplished by means of 1 mm thick glass slides. These slides were inclined slightly to prevent reflected light from returning back on the incident laser beam. They

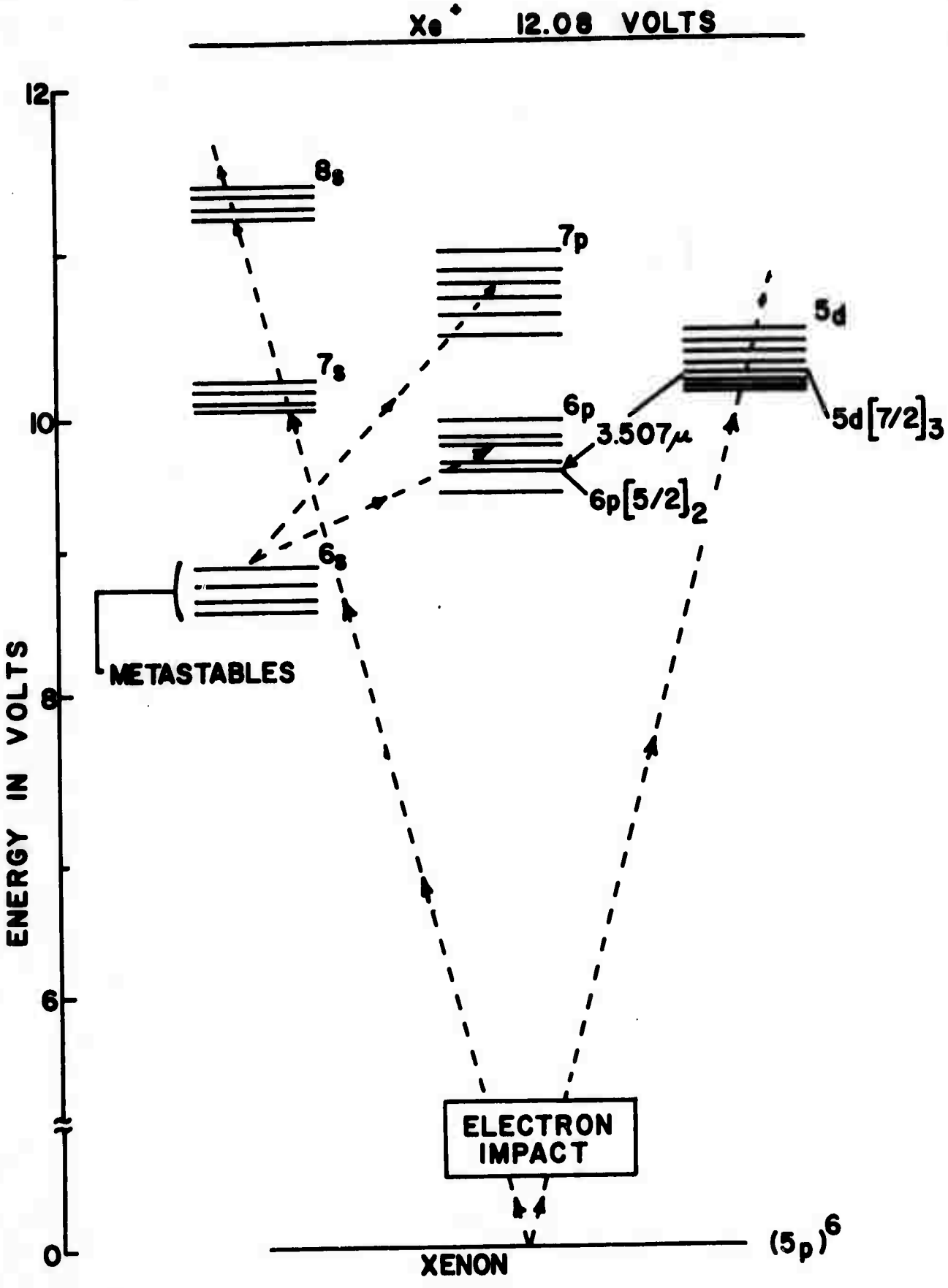

Fig. 18 - Xenon energy levels

were also alternately placed at opposite tilts during the run to minimize beam displacement through the amplifier. The beam was focused then recollimated to a plane wave with a cross sectional diameter approximately equal to the 1 cm diameter of the gain cell.

In order to monitor the input intensity, a beam splitter was positioned in front of the gain cell. This split the beam into a reference beam, and a signal beam which passed through the gain cell. The reference beam was then focused down and detected by means of a liquid nitrogen cooled InSb detector. Absolute intensity measurements were made with an Eppley thermopile. The thermopile was placed to intercept the signal beam, and the InSb detector was calibrated for intensity measurements.

The signal beam was passed through the gain cell, and detected, after being focused, by a liquid nitrogen cooled Ge:Au detector. The laser beam was modulated at 600 Hz by a chopper, which also provides a reference signal to a lock-in amplifier. The outputs of both detectors were examined by means of the lock-in amplifier. Normalization runs were made with the gain cell off. It was found that the ratio of the input beam to the output beam did not remain constant as the input beam was varied by four orders of magnitude. This can be attributed to a slight shift in the beam direction as the glass attenuators are placed in the path of the beam, or to a nonlinearity in one of the detectors. The change in the intensity ratio of the beams was not more than 25% as the intensity was varied. This error, however, is too large to tolerate. It was, therefore, necessary to normalize each reading, with the gain cell off, for each experimental point. The pressure in the gain cell was continuously monitored by means of an MKS Baratron capacitance manometer.

Before measurements were made, xenon discharges were run in the gain cell for long periods of time. This was done to imbed xenon in the walls and reduce variations in pressure as a result of subsequent adsorption. The data was taken by setting the Xe pressure and then measuring the gain as a function of input intensity. Results similar to those on SiF_4, as given in Fig. 10 were obtained. The small signal gain was found by extrapolating these results to low intensity. The saturation intensity was found in a similar fashion as with SiF_4; but because the medium exhibits gain rather than absorption, the results of Gordon, et al.,[16] were used.

The saturation intensity was measured at three xenon pressures: 20 mTorr, 30 mTorr, and 40 mTorr. At each pressure, measurements were made for different excitation currents. At the 30 mTorr and 40 mTorr pressures, at least one measurement was made when xenon exhibited absorption properties. The saturation intensity was found to be linear with pressure in this pressure range, and did not change, within experimental accuracy, for different discharge currents. The saturation intensity was found to be

$$I_s = 3.3 \pm 1\mu \text{ watt/cm}^2 - \text{mTorr} \quad . \tag{52}$$

The low value of the saturation intensity is consistent with the low output power of the He-Xe laser. The value of the saturation intensity agrees with an estimate derived from Clark's data on the amplification of Xe as a function of input power.[19] An estimate was made for the beam size in his experiment and the resulting saturation intensity was found to be of the same order of magnitude as the saturation intensity reported herein.

The variation of saturation intensity with respect to pressure was linear as could be expected from Eq. (28),

$$I_s = \frac{h^2 c \epsilon_o}{2T_1 T_2 \mu^2} \tag{53}$$

where T_1, the population relaxation time, is independent of pressure. Unlike a molecule, xenon does not have a reservoir of rotational states that can deplete the level population by collisional de-excitation. For pressures greater than 60 mTorr the saturation intensity could be reliably measured since its value is of the same order of magnitude as the intensity available from the He-Xe laser.

The results of gain measurements are shown in Fig. 19. To maintain clarity, only the experimental points for the 20 mTorr case is shown. The results were obtained by using an input intensity much smaller than the measured saturation intensity, and then recording the output intensity as the current in the Xe cell is varied. In each experimental run, the laser was first tuned to line center using the PZT stack. During a run the laser proved fairly stable, and the input intensity was monitored to insure a constant value.

At low discharge current, xenon exhibits gain. Except for the case of 20 mTorr pressure of xenon, absorption was observed at high currents. At currents in excess of 500 ma, the attenuation approached 10 dB/m. This behavior is consistent with the level populations approaching thermal equilibrium. It is assumed that at higher discharge currents, unattainable with the present apparatus, this result would hold for a pressure of 20 mTorr as well. The 30 mTorr case exhibits no maximum in the absorption; but for 35 mTorr, which is not included in Fig. 19, a maximum in absorption was seen.

These results are consistent with the theory presented in Section 4.1.

4.2.2 Xenon Lamb Dip Observations

In order to investigate the homogeneous width in xenon under conditions of absorption, and to determine the isotope shifts and hyperfine structure at 3.5μ, the "Lamb dip" was studied.

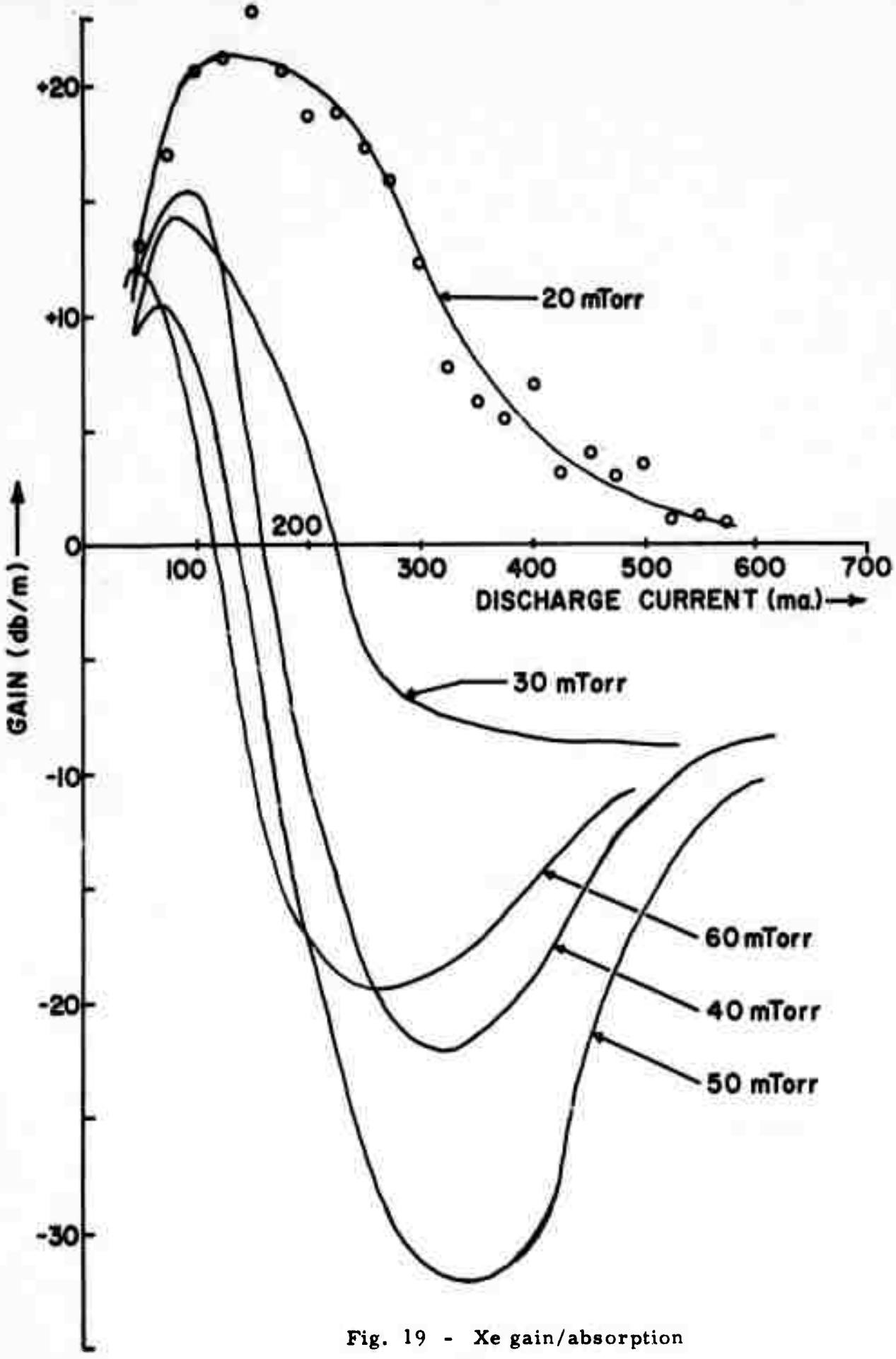

Fig. 19 - Xe gain/absorption

The experimental apparatus for the Lamb dip studies is shown in Fig. 20. The laser beam was collimated with a pair of spherical mirrors which were arranged so that the beam was nearly parallel to the optical axis to minimize astigmatism. The Lamb dip observations were made using two different techniques.

The first method is similar to that used with SiF_4. A chopper was placed between the laser and the attenuators and a reference signal from the chopper was applied to the lock-in amplifier. The oscilloscope sawtooth voltage was used in tandem with the dc supply to provide a linear and incremental voltage sweep for the PZT stack, which controlled the laser frequency. In this way a dip in the power was observed as a change in the dc output of the phase detector when the laser frequency was swept across the amplifying transition.

The second method used the configuration shown in Fig. 20. In this method, the laser was frequency modulated by applying a sine wave voltage, in addition to the sawtooth voltage, to the PZT. The sine wave voltage was also used as the reference frequency for the lock-in amplifier, and the signal was phase detected at the frequency of the sine wave. When the frequency modulated laser beam is double passed through the gain cell, the frequency modulation is converted into amplitude modulation by the variation in susceptibility across the line center. A discriminant is produced when the AM sidebands are phase detected. For small modulation frequencies compared with the homogeneous width, and small frequency deviations, this discriminant is approximately the first derivative of the Lamb dip as a function of frequency. This discriminant is superimposed on the discriminant due to the laser power tuning curve. The zero crossing of the Lamb dip discriminant is shifted when its frequency is not centered on the power tuning curve. Its height and peak-to-peak separation is related directly to the height and full width of the Lorentzian hole in the gain profile. The relationship for the width is

$$\Delta\nu\,(\text{Discriminant}) = \frac{1}{\sqrt{3}}\,\Delta\nu\,(\text{Lamb dip}) \quad . \tag{54}$$

Oscillograms of the central dip and its discriminant are shown in Figs. 21(a) and (b) respectively. Both oscillograms are with an Xe pressure of 11 mTorr. The horizontal scales are 4.26 and 3.4 MHz per division respectively. The lower trace on Fig. 21(a) is the calibration used to determine the frequency scale.

The Lamb dip discriminant observations are shown in Fig. 22. For convenience, the dips are labeled a, b, c, and d starting at lower frequencies, and this identification will be used in referring to a particular discriminant or dip. The relative frequency separations of the dips were measured by viewing the output of the lock-in amplifier on an oscilloscope. The full scale screen display on the oscilloscope, due to the sawtooth

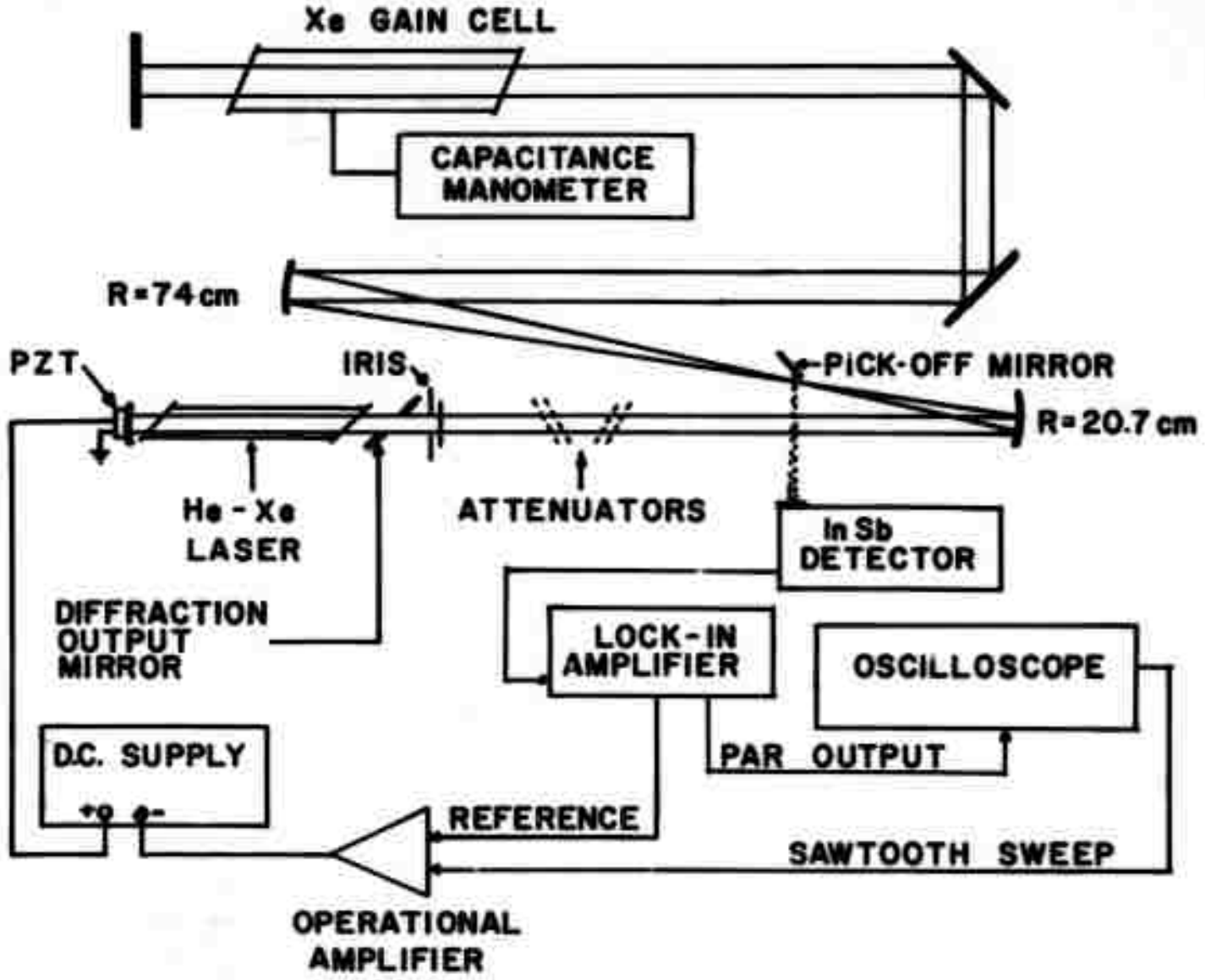

Fig. 20 - Xe Lamb dip discriminant apparatus

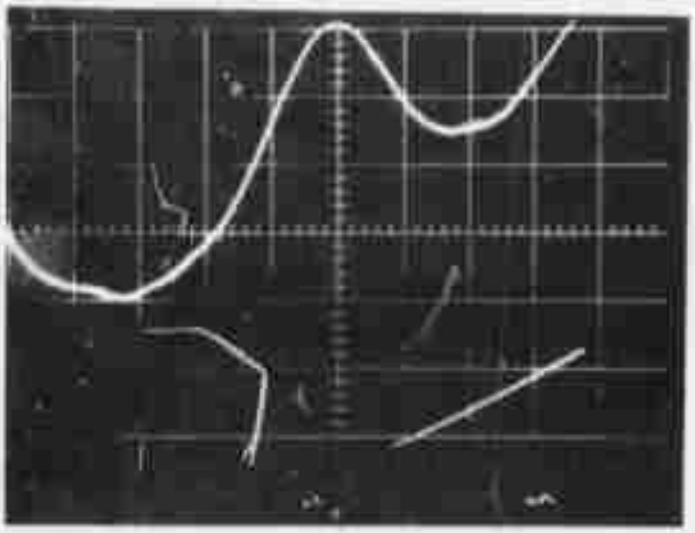

(a)

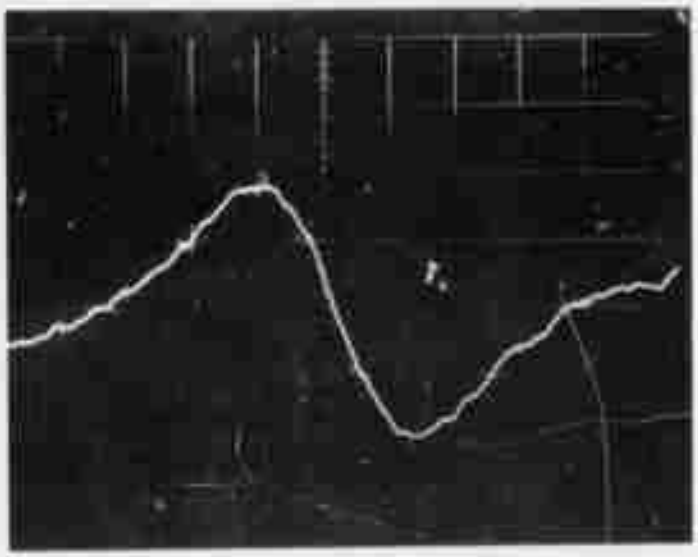

(b)

Fig. 21 - Xe Lamb dip and discriminant oscillograms

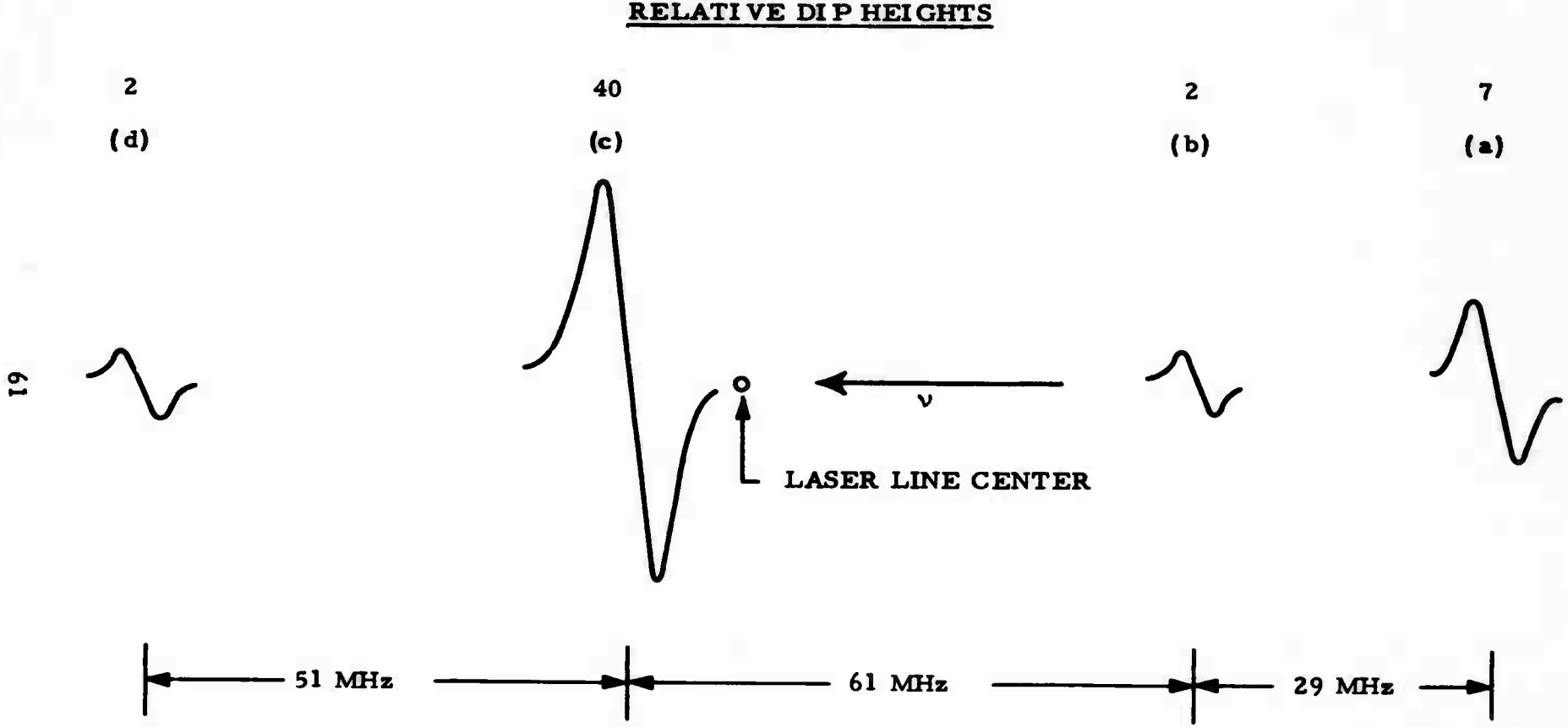

Fig. 22 - Xe Lamb dip observations

sweep, corresponds to a 34 MHz view of the Doppler line. The frequency separation between the (a) and (b) dip was determined by viewing both dips simultaneously. For the other separations a measurement of the frequency separation between the peak of one discriminant to a fiducial mark on the Doppler discriminant was made. A similar measurement between that fiducial mark and the adjacent discriminant's peak yielded the frequency separation. The separations are:

$$\Delta\nu(a - b) = 29 \pm 3 \text{ MHz}$$
$$\Delta\nu(b - c) = 61 \pm 10 \text{ MHz}$$
$$\Delta\nu(c - d) = 51 \pm 10 \text{ MHz} \quad .$$

The error is mainly due to hysteresis and nonlinearity in the PZT response.

The peak-to-peak heights of the discriminants are measured at a xenon pressure of 10 mTorr, and are in the ratio, a:b:c:d = 7:2:40:2. The absolute depth of the large dip (c) is measured to be approximately 3% of the peak power detected.

4.2.3 Interpretation of Lamb Dip Observations

The pressure dependence of the homogeneous width was studied for the large central Lamb dip (c). Oscillograms were taken for different xenon pressures and the input intensity was attenuated to keep from power broadening the dip. The result for the pressure broadening of the homogeneous width is 49 ± 20 kHz/mTorr, in the pressure range 5 to 50 mTorr. The resulting phase interruption time is found to be $T_2 = 6.55 \times 10^{-9}$ Torr-sec.

The zero pressure intercept for the pressure broadened width is theoretically the natural linewidth of the transition. This natural linewidth is found to be 9.8 MHz, yielding a spontaneous lifetime of 3.2×10^{-8} sec. This lifetime is in good agreement with the reported lifetime of 4.5×10^{-8} sec.[24]

The homogeneous widths of the other dips were measured at a pressure of 5m Torr of Xe. These dip widths are all smaller than the central dip width and all have approximately a 8.65 MHz homogeneous width. The resulting lifetime is 3.7×10^{-8} sec. Both of these widths agree closely with the 5 MHz "enhanced" Lamb dip width of Xe^{136} reported by Wang, et al.[21]

As indicated in Fig. 22, there is a frequency shift between the central dip (c) and the center of the power tuning curve. This is more evident from the asymmetry in Fig. 21(a). This shift is due to the change in the resonant transition of Xe, in the laser, due to collisions with helium atoms. These collisions perturb the energy levels of xenon and should be a function of the helium pressure. The frequency shift was measured for two different fills of the He-Xe laser. The measurement was made by displaying the double pass gain discriminant and the discriminant of the laser on a dual

beam oscilloscope. The second trace was obtained by splitting off part of the laser beam before it entered the gain cell and processing the signal derived from this beam in the same manner as the Lamb dip discriminant signal. The zero crossing of the double pass signal was frequency referenced with respect to the zero crossing of the unamplified beam, with the gain cell on and then off. This frequency difference yields the frequency shift between the laser central frequency and the Lamb dip. A crude check on these results can be made with the use of oscillograms similar to Fig. 19(a), showing the location of the Lamb dip relative to the power peak. The difficulty with this method involves the unraveling of the convolution of a Lorentzian with a Gaussian profile. The results for the frequency shift measurements are

Laser Fill	Frequency Shift
4 Torr-He; 0.06 Torr-Xe	6.8 MHz
8 Torr-He; 0.1 Torr-Xe	14.5 MHz

The frequency shift is to lower frequency. There is no Xe-Xe shift observed as the pressure in the gain cell is varied.

All Lamb dips and discriminant observations were made with xenon as an amplifier. At a pressure of 30 mTorr, the discriminant could be clearly seen at a discharge current of 100 ma. As the current was increased the signal became very noisy. At 400 ma, where the maximum absorption occurs, the discriminant could not be observed. Other pressures were tried with the result that neither the dip nor discriminant was observed when the xenon was absorbing. However, the signal-to-noise ratio was very poor.

5.0 CONCLUSIONS AND RECOMMENDATIONS

5.1 Conclusions

A BALAD receiver for 10.6μm CO_2 laser signals with the specifications listed in Section 5.2 is feasible for application in an optical radar. Its usefulness would be to detect a target of uncertain position. For example, the receiver could be remote from the transmitter. It could also sensitively receive several separated signals simultaneously, or even an entire image.

A BALAD receiver utilizing xenon gas could function in a shorter range but higher resolution optical radar than the CO_2 system. This wide-angle receiver also could be utilized in a lightweight secure communication system.

5.2 Achievable BALAD Receiver

Using the data in Table 2 and the known characteristics of CO_2 and Xe amplifiers, it is possible to compute sets of BALAD receiver characteristics. Use is made of the theory summarized in Sections 2.1 and 2.2, and given in detail in the previous report.

Examples of such specifications are given in Table 3. It is assumed that the optical waveguide or fly's eye lens train configurations are used for both the amplifier and the absorber (see Sections 1.4 and 2.2).

As was noted in Section 2.1, the detection error rates are primarily determined by the input pulse statistics and are little affected by other considerations. In effect, the quantum efficiency of the receiver is close to 100%.

The respectable 1 watt of peak signal output power at $\lambda = 10.6\mu m$ makes possible a heterodyne Doppler measurement without requiring an array of detectors and circuits. If a weak local oscillator is used over the whole field-of-view, a negligible amount of noise will be introduced. This would be accomplished by inverting the power ratio of signal and local oscillator, that is, by interchanging their roles in the heterodyne detection process.

The 1 watt of average power[25] which is presently available at $\lambda(Xe) = 3.5\mu m$ does not allow a range comparable to a CO_2 laser radar. However, shorter range but higher-resolution radars and communication systems are possible with relaxed aiming requirement.

5.3 Recommendations

Additional work on the following tasks are recommended for the further development of the BALAD receiver.

a) The "fly's eye" and optical waveguide absorber configurations should be further investigated with a view to determining fabrication and experimental procedure.

Table 2. Key Characteristics of Saturable Absorbers in BALAD Receivers

Gas	Absorption Coefficient, α_o	Homogeneous Saturation Bandwidth, B	Saturation Intensity, I_s	Figure-of-Merit $F_M \equiv [\alpha_o B/I_s]$
CO_2	$0.7 \frac{(\text{meter})^{-1}}{\text{torr}}$	$7 \times 10^6 \frac{\text{hertz}}{\text{torr}}$	$5 \times 10^4 \frac{\text{watts}}{\text{m}^2\text{torr}^2}$	$1.0 \times 10^2 \frac{\text{meter}}{\text{joule}}$
SiF_4[a]	30	5×10^6	3.5×10^4	4.2×10^3
SF_6(300°K)[b]	130	21×10^6	7×10^4	3.9×10^4
SF_6(130°K)[b]				3.1×10^5
Xe(discharge)[c]	(70m^{-1})[c]	$(10^7$ hertz)[c]	$(1 \frac{\text{watt}}{\text{meter}^2})$[c]	(5×10^8)[c]

a. coincidence with the P-36 line of the 9.6μm CO_2 group.

b. coincidence with the P-16 line of the 10.7μm CO_2 group. The vapor pressure at 130°K is approximately 0.05 torr.

c. These approximate values are for the xenon 3.5μm transition in a discharge excited within a 0.5 mm diameter glass tube.

Table 3. Possible BALAD Receiver Characteristics (optical waveguide or fly's eye configuration)

	CO_2 laser-P(16) line @ 10.6μm SF_6 absorber @ 130°K	Xenon laser @ 3.5μm Xe discharge absorber
input signal pulse	150 photons	150 photons
pulse length	0.3μ sec	0.3μsec
input signal power	10^{-11} watt	3×10^{-11} watt
pulse bandwidth	1 MHz	1 MHz
amplification bandwidth (signal frequency range)	30 MHz	100 MHz
field-of-view (signal direction range)	100 x 100 resolution elements (2 deg. x 2 deg.)	200 x 200 res. elements (4 deg. x 4 deg.)
pulse error rates no-detection rate false alarm rate	 10^{-16}/pulse $\ll$ 1/year	 10^{-16}/pulse $\ll$ 1/year
Max. signal amplification	100 dB	110 dB
Max. peak signal to detector relative background attenuation effective quantum efficiency	1.0 watt 50 dB $\gtrsim$ 75%	0.003 watt 55 dB $\gtrsim$ 75%
amplifier-absorber length	5 meter	1 meter
amplifier-absorber diam.	10 cm	10 cm
focused spot diam.	1 mm	0.5 mm

b) An experimental test of the BALAD receiver principle should be carried out using Xe-Xe media or CO_2-SF_6 media. The latter would be somewhat more expensive.

c) An investigation should be made of techniques for filtering out spontaneous emission from all but the working CO_2 laser line.

d) The theoretical analysis of the propagation of short pulses in strongly absorbing (or amplifying) laser media should be extended.

References

1. G. Gould, et al., RADC TR-72-110, 14 April 1972.
2. G. Gould, Proposal to ARPA, "Investigation of Low Noise Laser Receiver."
3. P. W. Smith, Appl. Phys. Lett. 19, 132 (1971).
4. J. T. Bridges, E. G. Burkhardt, and P. W. Smith, Appl. Phys. Lett. 20, 403 (1972).
5. A. Yariv, "Quantum Electronics," (John Wiley, New York, 1967), Chapt. 14.
6. G. Lamb, Rev. Modern Phys. 43, 99 (1971).
7. S. L. McCall and E. L. Hahn, Phys. Rev. 183, 457 (1969).
8. S. L. McCall and E. L. Hahn, Phys. Rev. A2, 861 (1970).
9. F. A. Hopf and M. A. Sculley, Phys. Rev. 179, 399 (1969).
10. A. Icesevgi and W. E. Lamb, Jr., Phys. Rev. 185, 517 (1969).
11. L. A. Gribov, "Intensity Theory for Infrared Spectra of Polyatomic Molecules," Academy of Sciences Press, Moscow (1963) Translation (Library of Congress Catalog Card Number 64-17204).
12. G. Hertzberg, "Infrared and Raman Spectra of Polyatomic Molecules," D. Van Nostrand Co., New York (1945).
13. H. Brunet and M. Perez, J. Molecular Spectroscopy 29, 472 (1969).
14. F. Shimizu, Appl. Phys. Lett. 14, 378 (1969).
15. P. Rabinowitz, "Lamb Dip Spectroscopy and CO_2 Frequency Stabilization on SF_6," AFOSR Scientific Report No. PIB EP-70-065 (1970).
16. E. I. Gordon, A. D. White, J. D. Rigden, "Gain Saturation at 3.39μ in the He-Ne Maser," MRI Symposium Proceedings XIII, Optical Masers (New York: Polytechnic Press, 1963).
17. N. Djew and G. J. Wolga, J. Appl. Phys. 42, 3226 (1971).
18. "Handbook of Chemistry and Physics," Chemical Rubber Publishing Co., Cleveland, Ohio (1955).
19. P. O. Clark, J. Quant. Elect. QE-1, 109 (1965).
20. R. Targ, et al., Appl. Phys. Lett. 17, 305 (1970).
21. Wang, et al., Appl. Phys. Lett. 17, 120 (1970).
22. F. Horrigan, "Xenon Laser Research," AFAL-TR-65-221 (1966).
23. W. R. Bennett, Appl. Optics - Supplement 2 - "Chemical Lasers," (1965), p. 3.
24. Allen, et al., J. Opt. Soc. Am. 59, 852 (1969).
25. R. Targ and M. W. Sasnett, J. Quant. Elect. QE-8, 166 (1972).